OSSERVAZIONI

AMMASSI DI GALASSIE

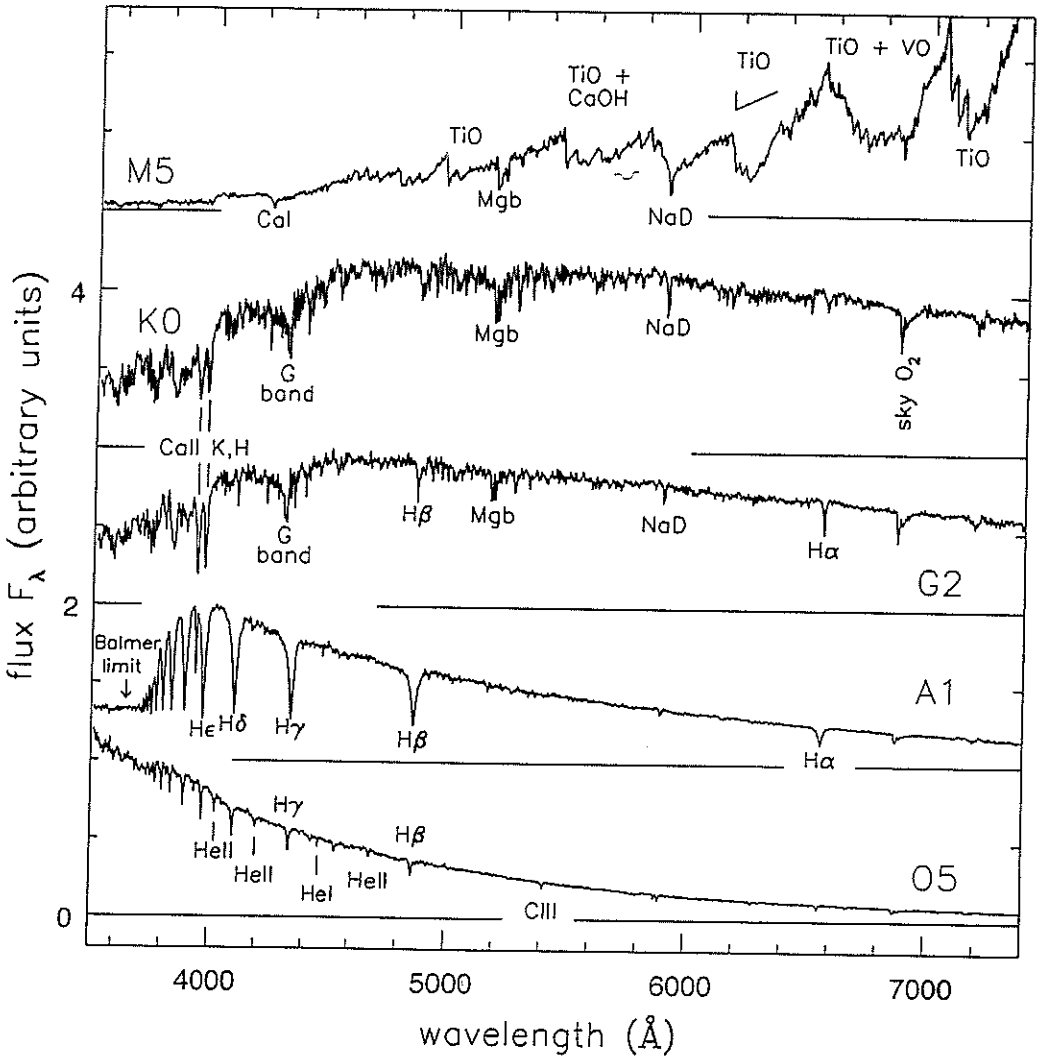

Figure 1.1 Optical spectra of main-sequence stars with roughly the solar chemical composition. From the top in order of increasing surface temperature, the stars have spectral classes M5, K0, G2, A1, and O5 – G. Jacoby *et al.*, spectral library.

The temperatures of O stars exceed 30 000 K. Figure 1.1 shows that the strongest lines are those of HeII (once-ionized helium) and CIII (twice-ionized carbon); the Balmer lines of hydrogen are relatively weak because hydrogen is almost totally ionized. The spectra of B stars, which are cooler, have stronger hydrogen lines, together with lines of neutral helium, HeI. The A stars, with temperatures below 11 000 K, are cool enough that the hydrogen in their atmospheres is largely neutral; they have the strongest Balmer lines, and lines of singly ionized metals such as calcium. Note that the flux decreases sharply at wavelengths less than 3800 Å; this is called the *Balmer jump*. A similar *Paschen jump* appears at wavelengths that are $3^2/2^2$ times longer, at around 8550 Å.

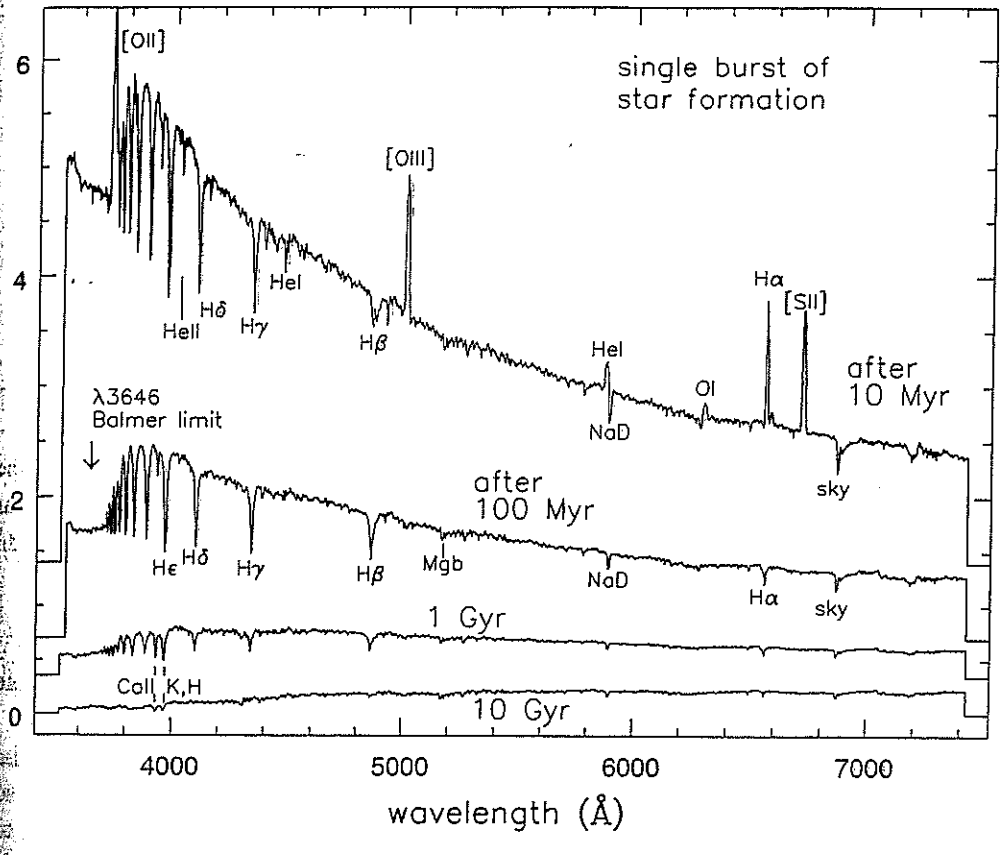

Figure 6.19 Spectra for a 'galaxy' that makes its stars in a 10^8 yr burst, all plotted to the same vertical scale. Emission lines of ionized gas are strong 10 Myr after the burst ends; after 100 Myr, the galaxy has faded and reddened, and deep hydrogen lines of A stars are prominent. Beyond 1 Gyr, the light dims and becomes slightly redder, but changes are much slower – B. Poggianti.

big ellipticals are richer in heavy elements than the midsized ones. The center of a galaxy is also more metal rich than its periphery: Figure 6.20 shows that the magnesium absorption is stronger, the greater the speed required for material to escape from that region of the galaxy. Smaller galaxies may have lost most of their metal-enriched gas, while larger systems were able to trap theirs, incorporating the heavy elements into new stars. Figure 1.5 showed us that metal poor stars of a given mass are bluer, especially while they are burning helium in their cores; so we are not surprised to find that smaller galaxies with lower metal content are bluer.

The most metal-rich parts of galaxies in Figure 6.20 correspond to abundances of 1–2 $Z_\odot$; stars at the center of luminous ellipticals are at least as metal-rich as the Sun. But they do not contain heavy elements in the same proportions as the Sun. Relatively light atoms such as oxygen, sodium, and magnesium are a few times more abundant relative to iron. We saw the same pattern in old metal-poor

File: p.fits JulDate: 2452199.54165

Object:A209 RA: 22:57:36.14 DEC: -13:37:38.0 2000.0

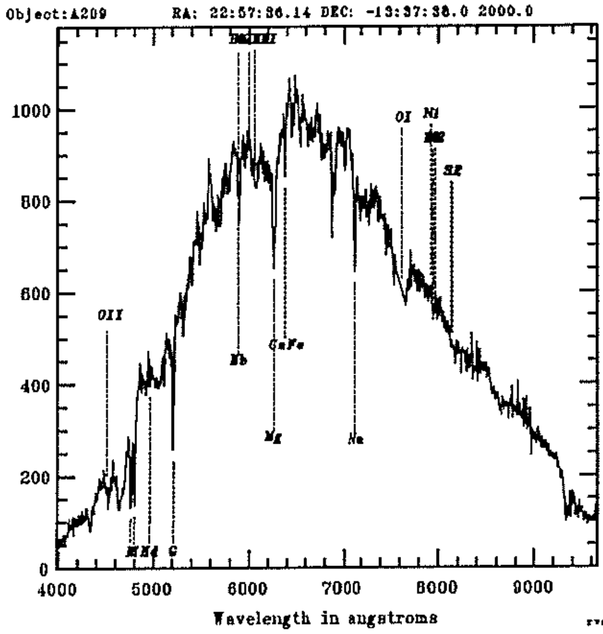

rvsao.xcsao 2.2.4 03-Jun-2002 14:06

2001-Oct-17 00:00:00.00

Object file BCV: 0.000

VELOCITY = 62882.88 +- 32.79 km/sec _

*Corr vel = 62882.88 +- 29.15 km/sec R= 20.7

Emis vel = INDEF +- INDEF km/sec 0/0 lines

Template	CZ	error	R
m0ix_E	62882.875	29.193	20.74
kenn_EL	62870.412	34.095	18.08
kenn_S0	62899.875	32.615	17.51
m01	62856.376	38.783	15.08
kenn_Sb	62884.145	47.133	11.35
kenn_Sa	62900.920	48.845	10.38
star	64099.982	80.464	8.86
kenn_Sc	62782.316	78.235	6.89
kenn_Ir	62840.212	119.882	8.14

No emission lines found?

cD GALAXY

deep Hδ

E+A GALAXY

POST-STARBUST GALAXY?

File: p.fits JulDate: 2452199.54165

Object:A209 RA: 22:57:36.14 DEC: -13:37:38.0 2000.0

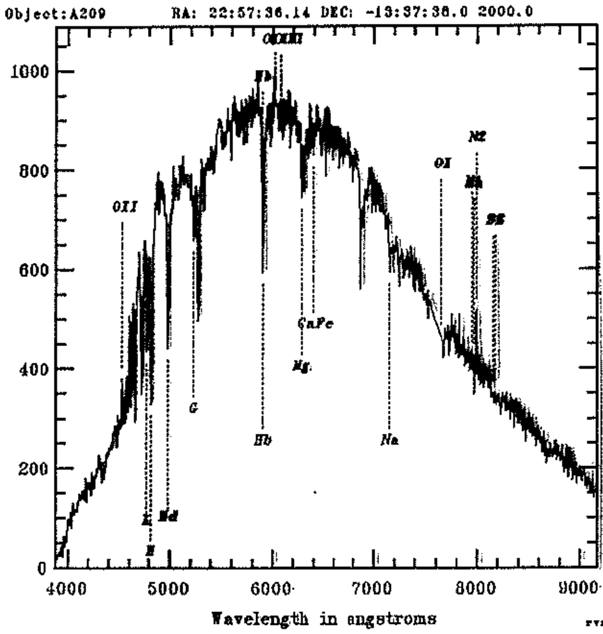

rvsao.xcsao 2.2.4 03-Jun-2002 14:05

2001-Oct-17 00:00:00.00

Object file BCV: 0.000

VELOCITY = 64178.58 +- 38.38 km/sec _

*Corr vel = 64178.58 +- 29.48 km/sec R= 17.9

Emis vel = INDEF +- INDEF km/sec 0/0 lines

Template	CZ	error	R
kenn_Ir	64178.577	29.480	17.91
kenn_Sc	64214.885	29.680	17.78
kenn_Sb	64421.738	40.374	11.28
kenn_Sa	64398.690	57.082	8.50
kenn_S0	64405.941	58.804	7.38
kenn_EL	64502.840	80.409	6.02
m0ix_E	64462.081	88.604	5.39
m01	64351.272	92.847	4.78
star	68457.276	433.061	2.58

No emission lines found?

File: p.fits JulDate: 2452201.52465

Object:A209 RA: 23:01:08.56 DEC: -13:38:46.2 2000.0

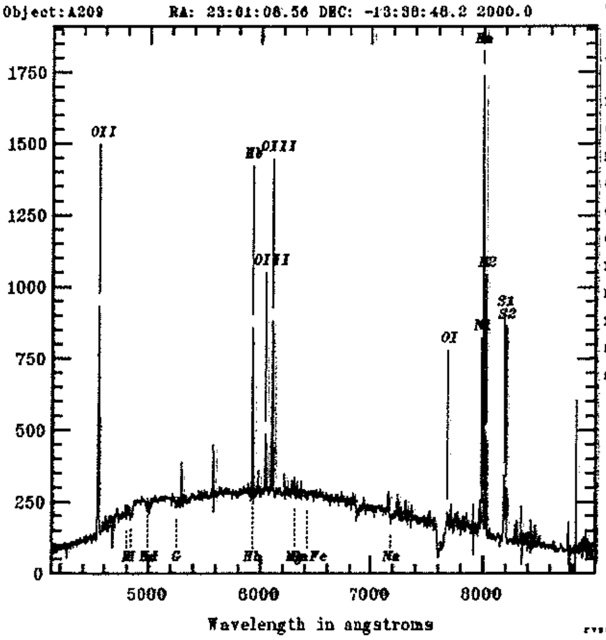

rvsao.emsao 2.2.4 03-Jun-2002 14:10

2001-Oct-19 00:00:00.00

Object BCV: 0.000

VELOCITY = 65619.95 +- 19.64 km/sec _

*Emis vel = 65619.95 +- 12.71 km/sec 10/10 l

Line	Rest	Obs.	CZ	error
OII	3727.30	4549.37	65630.10	12.88
Hb	4861.33	5925.41	65679.30	12.62
OIII	4958.91	6044.71	65642.14	39.47
OIII	5006.84	6102.90	65632.06	9.84
OI	6300.30	7678.93	65694.62	15.97
N1	6548.06	7981.04	65608.56	382.1
Ha	6562.82	7999.15	65612.35	8.34
N2	6583.57	8024.83	65616.26	22.24
S1	6716.44	8186.29	65607.71	12.16
S2	6730.81	8204.08	65610.77	10.11

EMISSION LINE GALAXY

... STARBUST?

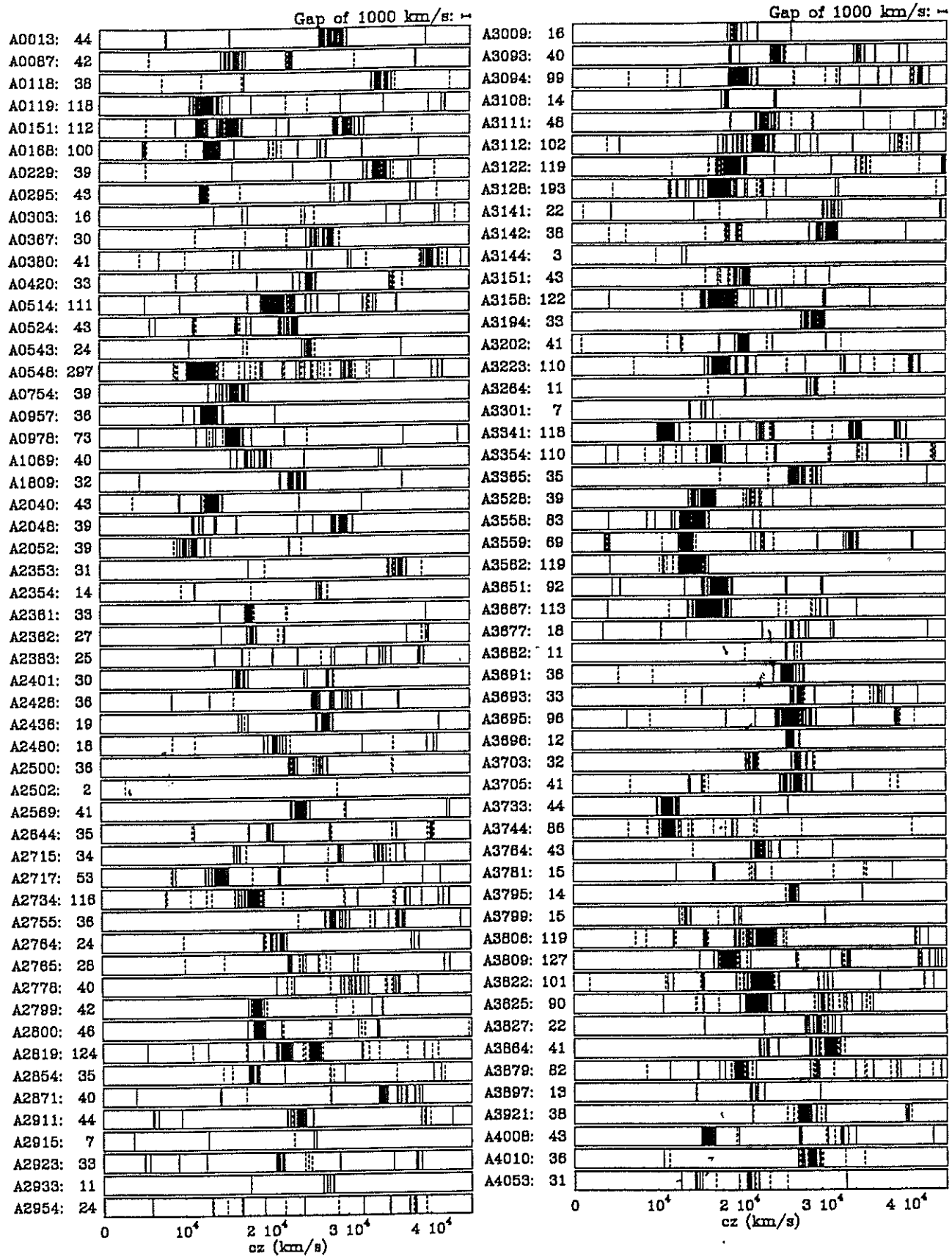

Fig. 7. Distribution of radial velocities in the directions of the 107 target ACO clusters studied in the ESO Nearby Abell Cluster Survey (ENACS). Solid bars indicate velocities derived solely from absorption lines, dashed bars indicate velocities derived from emission lines or from emission and absorption lines. The total number of galaxy redshifts in a survey is shown next to the Abell number of the cluster.

Selection of Cluster Members

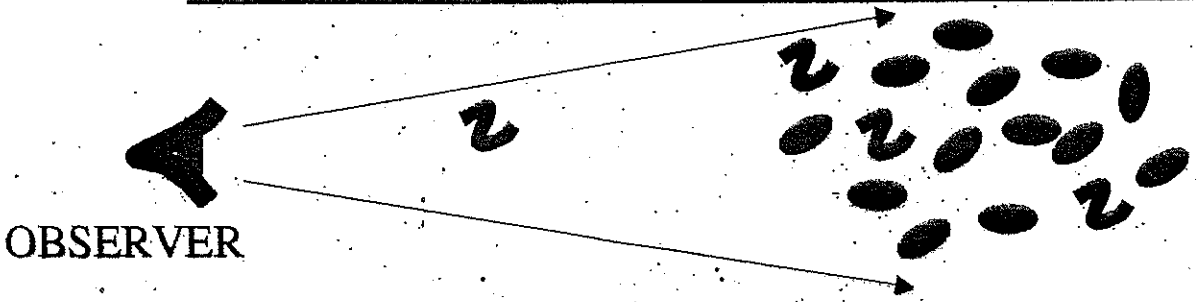

Coma cluster region
Palomar Sky Survey plate

Density peaks in the velocity distribution (adaptive kernel method; Pisani 1993; MG et al. 1996).

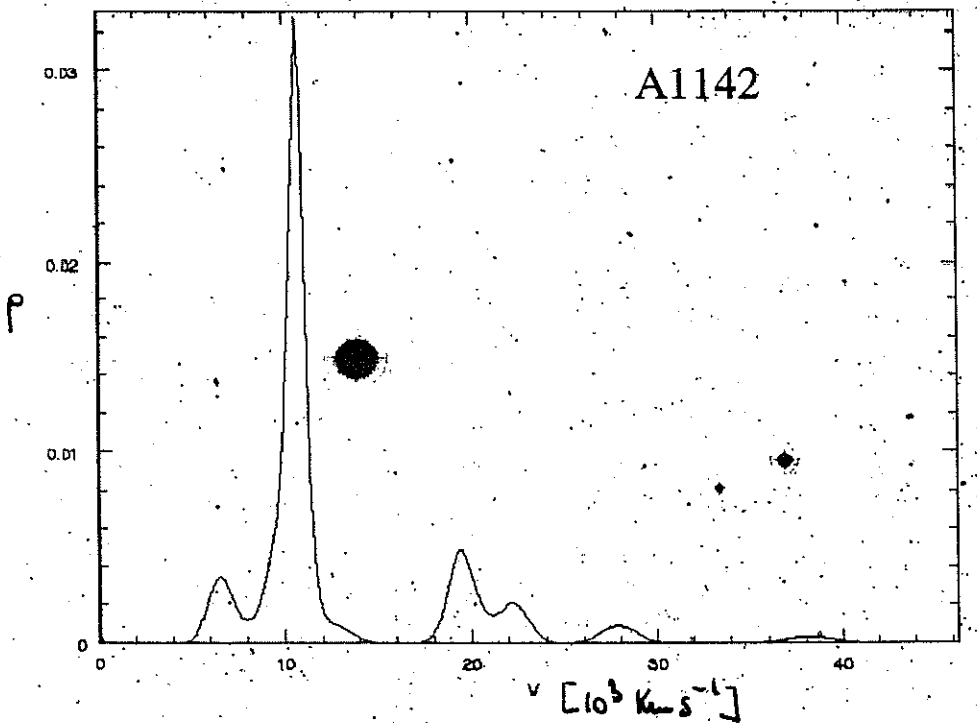

Velocity+position information (shifting gapper; Fadda et al. 1996).

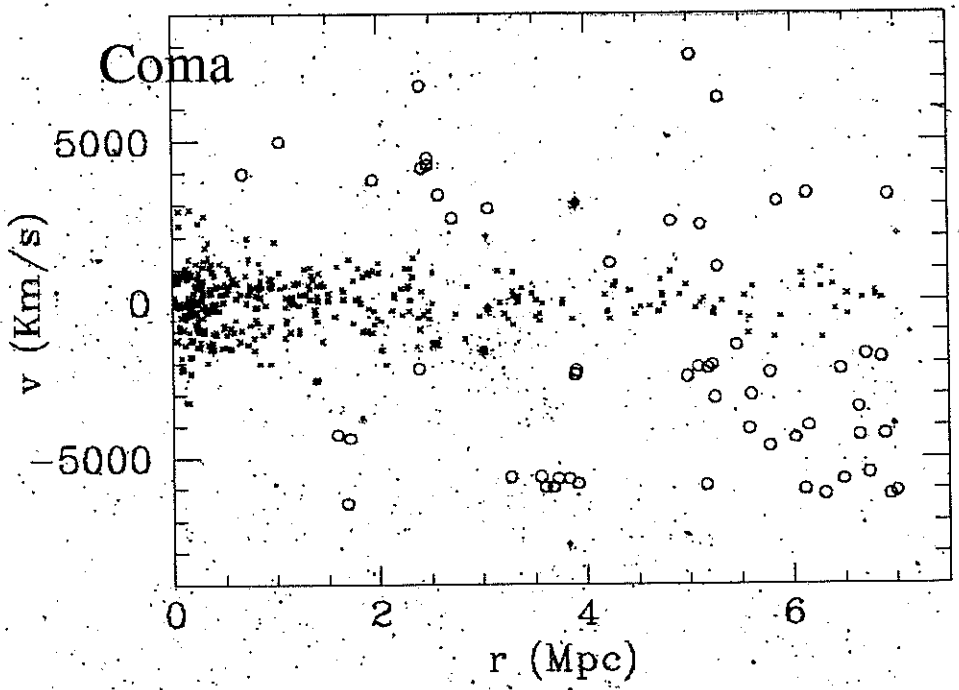

GIRARDI ET AL. IN PREP. 2007

ANALISI DI SIMULAZIONI N-BODY (BORGANI ET AL.)

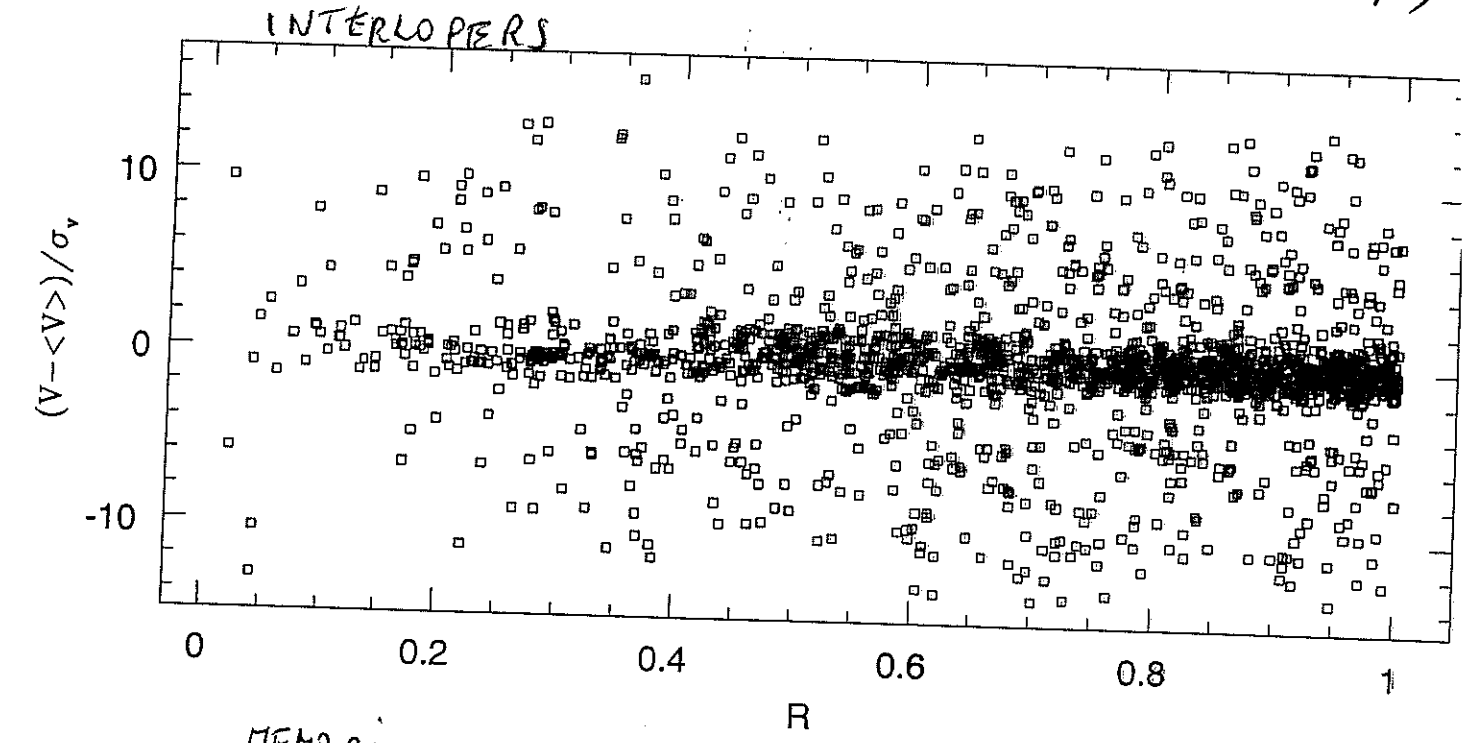

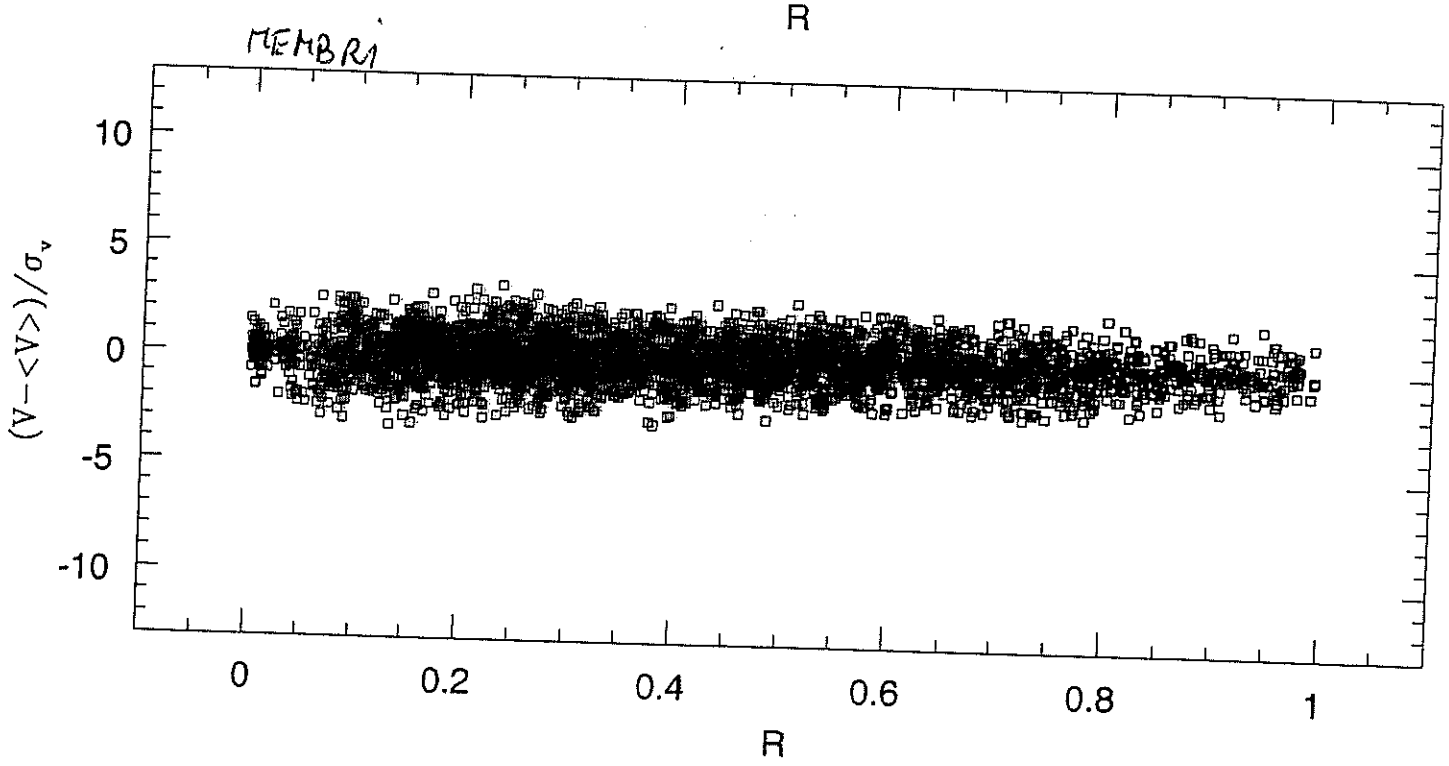

β problem CFR. FRA σ_v e T_x

Eq. dell'eq. idrostatica x gas ICM

μ = peso molecolare medio ~ 0.58
m_p = massa protone

$$\frac{d\phi}{dr} = \frac{GM(r)}{r^2} = -\frac{1}{\rho}\frac{dP_{gas}}{dr} = -\frac{1}{\rho}\frac{d}{dr}\left(\frac{\rho KT}{\mu m_p}\right)$$

$$\frac{GM(r)}{r^2} = -\frac{1}{\rho}\frac{K}{\mu m_p}\left(\rho\frac{dT}{dr} + T\frac{d\rho}{dr}\right)$$

$$M(r) = -\frac{kT}{G\mu m_p}\cdot r\left[\frac{d\ln\rho}{d\ln r} + \frac{d\ln T}{d\ln r}\right]$$

Osservativamente uso x il fit il modello "isotermo" - β model (Cavaliere e Fusco Femiano 76)

$$\rho_x(r) = \rho_{0x}\left(1 + \left(\frac{r}{r_{0x}}\right)^2\right)^{-3/2\,\beta_{fit,gas}}$$

$$\Sigma_x(R) = \Sigma_{0,x}\left(1 + \left(\frac{R}{r_{0x}}\right)^2\right)^{-\beta_{fit,gas}}$$

emissività $\propto \rho^2 \Rightarrow$ surface brightness $S_x = S_{0x}\left(1+\left(\frac{R}{r_{0x}}\right)^2\right)^{-3/2\,\beta_{fit,gas}+1/2}$

gas - X
Bremsstrahlung

X galassie in Ammesso

$$M(r) = -\frac{\sigma_r^2 r}{G}\left[\frac{d\ln\rho}{d\ln r} + \frac{d\ln\sigma_r^2}{d\ln r} + 2\beta\right]$$

$\beta(r)$ = parametro di anisotropia di vel. $= \left(1 - \frac{\sigma_\theta^2}{\sigma_r^2}\right)$

Osservativamente

$$\rho(r) = \rho_0\left(1+\left(\frac{r}{r_0}\right)^2\right)^{-3/2\,\beta_{fit\,gal}}$$

$$\Sigma(r) = \Sigma_0\left(1+\left(\frac{R}{r_0}\right)^2\right)^{-\beta_{fit\,gal}}$$

modello di King modificato
(modello di King x Ammesso ha $\beta_{fit\,gal} = 1$
$\rho \propto r^{-3}$
$\Sigma \propto r^{-2}$)

Confronto tra $M(r)$ da X (ICM) e da pols.

ASSUNTO ENTRAMBI ISOTERMI

(~ OK con osservazioni)

$$-\frac{kT}{\mu m_p}\frac{d\ln\rho_x}{dr} = -\sigma_r^2\frac{d\ln\rho}{dr} - \frac{2\beta\sigma_r^2}{r}$$

$$\frac{\frac{d\ln\rho_x}{dr}}{\frac{d\ln\rho}{dr}+\frac{2\beta}{r}} = \boxed{\frac{\sigma_r^2}{\frac{kT}{\mu m_p}} \equiv \beta_{spec}}$$

β spettroscopico

$$\beta_{spec} \equiv \frac{\sigma^2_{LOS}}{\frac{kT}{\mu m_p}}$$

$\sigma_r^2 \simeq \sigma^2_{LOS}$ SU MISURE GLOBALI

Uso profili di ρ usati osservativamente $\times$ fit

$\times$ r grandi $\gg r_0$

$$\beta_{spec} = \frac{-3\beta_{fit,gas}\cdot\frac{1}{r}}{-3\beta_{fit,gas}\cdot\frac{1}{r} - \frac{2\beta}{r}} = \frac{\beta_{fit,gas}}{\beta_{fit,gas} - \frac{2}{3}\beta}$$

Osservativamente: β_{spec} è $\gg 1$, $\sigma_r^2 \sim \sigma^2_{LOS}$

Storicamente: $\beta_{fit,gas} \sim \frac{2}{3} \sim 0{,}677\ldots$, $\beta_{fit,gal} \sim 1$, $\beta \sim 0$ (almeno $\times$ gals vale è vero!)

β problem !!! $\sim \frac{2}{3}$

Superato negli anni 90

Migliori misure (meno interlopers!) σ^2_{LOS} (ed anche T_x) $\Rightarrow$ $\beta_{spec} \lesssim 1$

$\beta_{fit,gal} \sim 0{,}8 \Rightarrow \frac{\beta_{fit,gas}}{\beta_{fit,gal}} \sim \frac{2/3}{0{,}8} \lesssim 1$ ok!

β problem (I)

$$\beta_{spec} = \frac{\sigma^2_{LOS}}{\frac{KT}{\mu m_p}} = 1$$

Aspettato se gals e gas "cadono" assieme nella buca di potenziale formata da DM (es. Sarazin 1986 review)

cioè = energia x unità di massa

"infall comune" di gas e gals

invece:

osservativamente: prima del 1990 $\beta_{spec} >> 1$

con osservazioni migliori $\beta_{spec} \leq 1$ → x Ammassi poveri o gruppi

Perchè? È vero? Problema ancora irrisolto!

Possibili spiegazioni:

1) frizione dinamica ed effetti successivi all'infall + importanti x gruppi

2) gas scaldato da AGN in gruppi riesce a far aumentare T

[illegible]

3) problema di pochi oggetti/gals. nei gruppi: difficile stimare σ_{LOS}!

Velocity Dispersion and X-ray Temperature

(with Fadda, Giuricin, Mardirossian, Mezzetti, Biviano 1996, ApJ 457, 61).

T_X from David et al. (1993).

37 nearby clusters with reliable σ_v:

$$\sigma_v = 10^{2.53\pm0.04} \times T_X^{0.61\pm0.05}$$

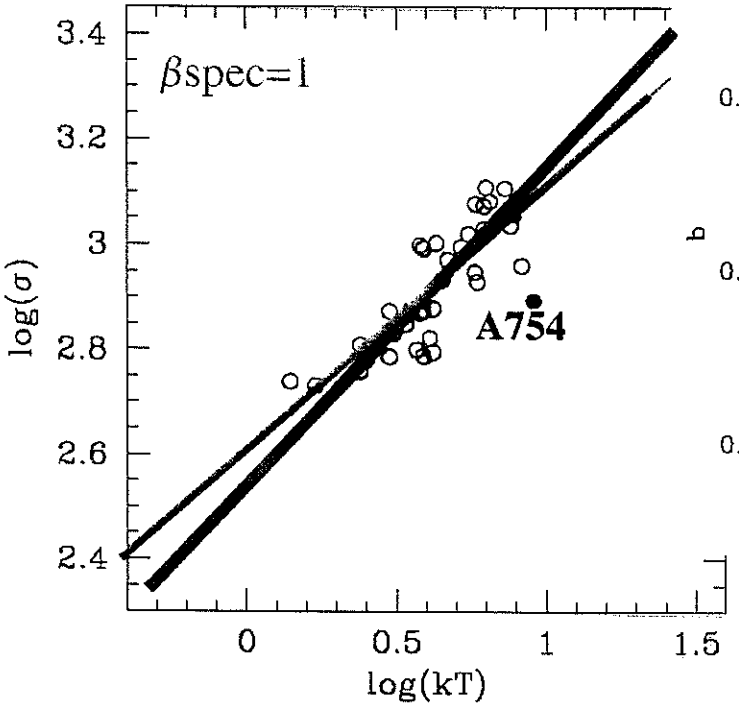

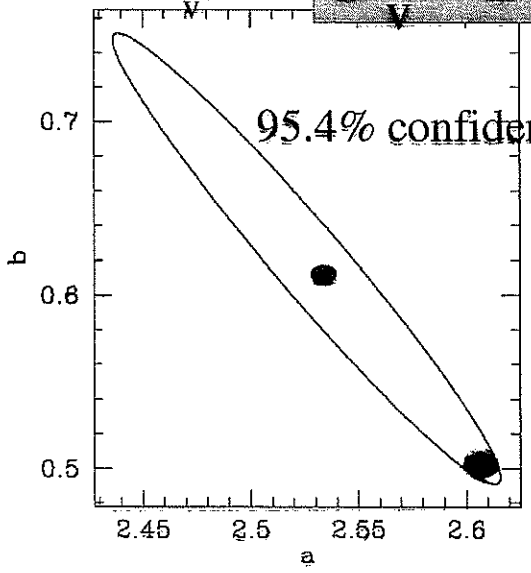

$$\sigma_v = 10^{2.51\pm0.03} \times kT^{0.62\pm0.04}$$

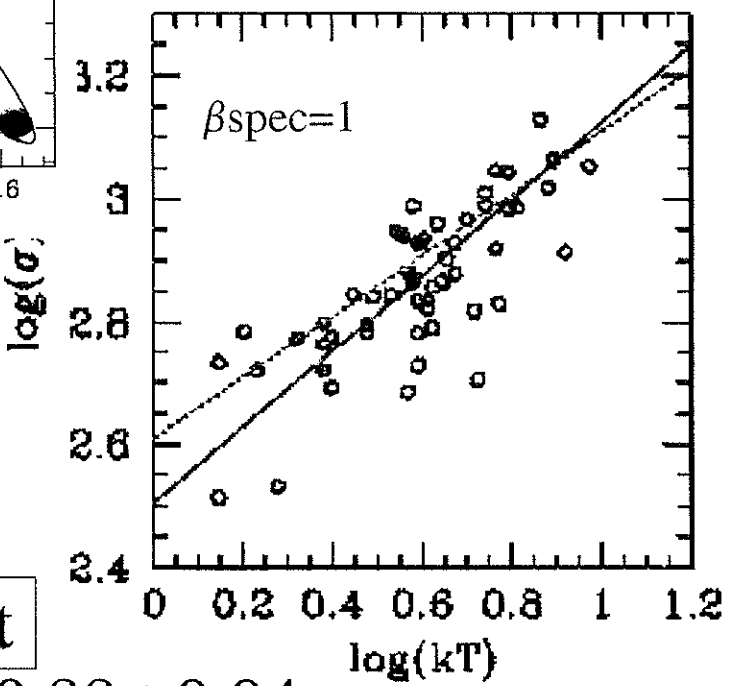

(coll. with Giuricin, Mardirossian, Mezzetti, and Boschin 2000, ApJ 505, 74; 55 clusters)

No longer consistent model of perfect gals/ICM energy equipartition! $\beta_{spec} = 0.88 \pm 0.04$

DET. DELLE ANISOTROPIE DI VELOCITÀ DELLE ORBITE DELLE GALS IN AMMASSO

Integral VDP velocity dispersion profile

Analytical models for cl. TEORIA

based on the JEANS Eq. (e.g. Merritt 87)

same Φ potential
same T kinetic energy

$\sigma_{obs}(r_i)$ profile

anisotropy parameter

isotropic case
$\beta = 0$

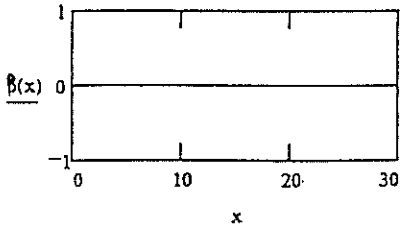

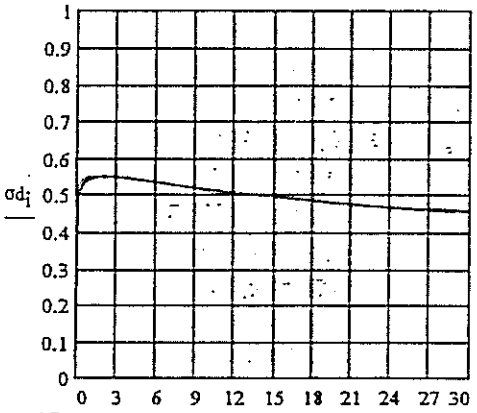

$$\beta(r) = \frac{r^2}{r^2 + r_0^2}$$ velocity anisotropy

$r_i = \frac{r}{r_c}$ r_i (projected distance)

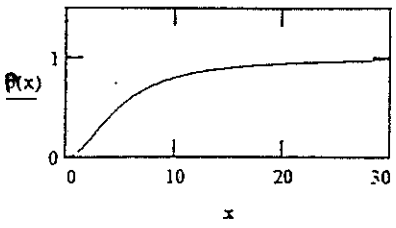

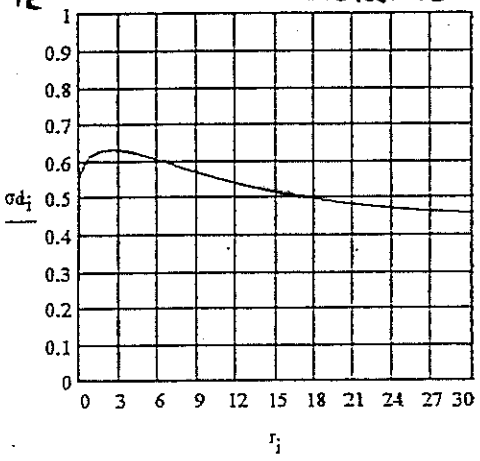

external radial orbits
$\beta > 0$

$\beta = 1$ completely radial

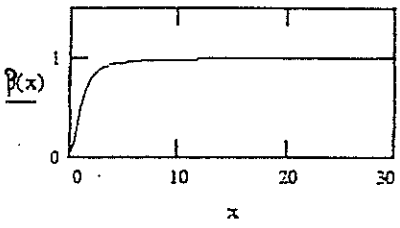

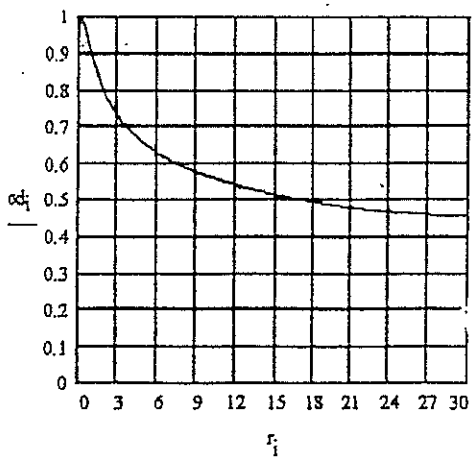

To avoid possible velocity anisotropies we have to adopt the global σ_{los} !

related to the total gravitational potential

Integral Velocity Dispersion Profiles and Velocity Anisotropies

DATI

(MG et al. 1996, Fadda et al. 1996, MG et al. 1998)

Analysis of integral velocity dispersion profile of nearby clusters.
Velocity anisotropies+ DM distribution⇒trend of profiles

Possible anisotropies do not affect global estimate: a flat profile in external region ⇒no longer effect of anisotropies.

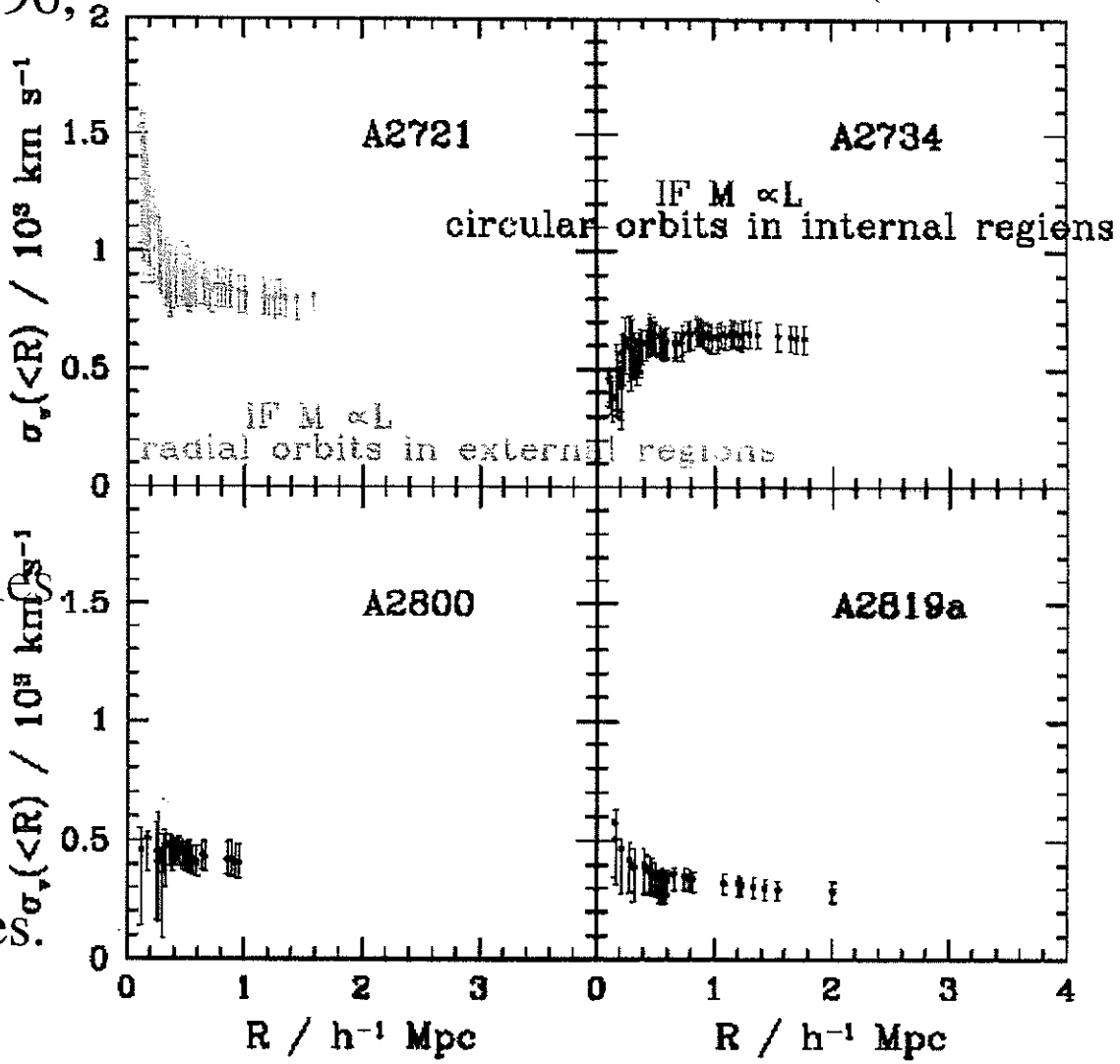

Velocity Dispersion Profiles

DISTANT CLUSTERS

The behaviour of σ_v profiles
is consistent with that of nearby clusters

BUT... some clusters suffer for the poor sampling
and/or small spatial extension

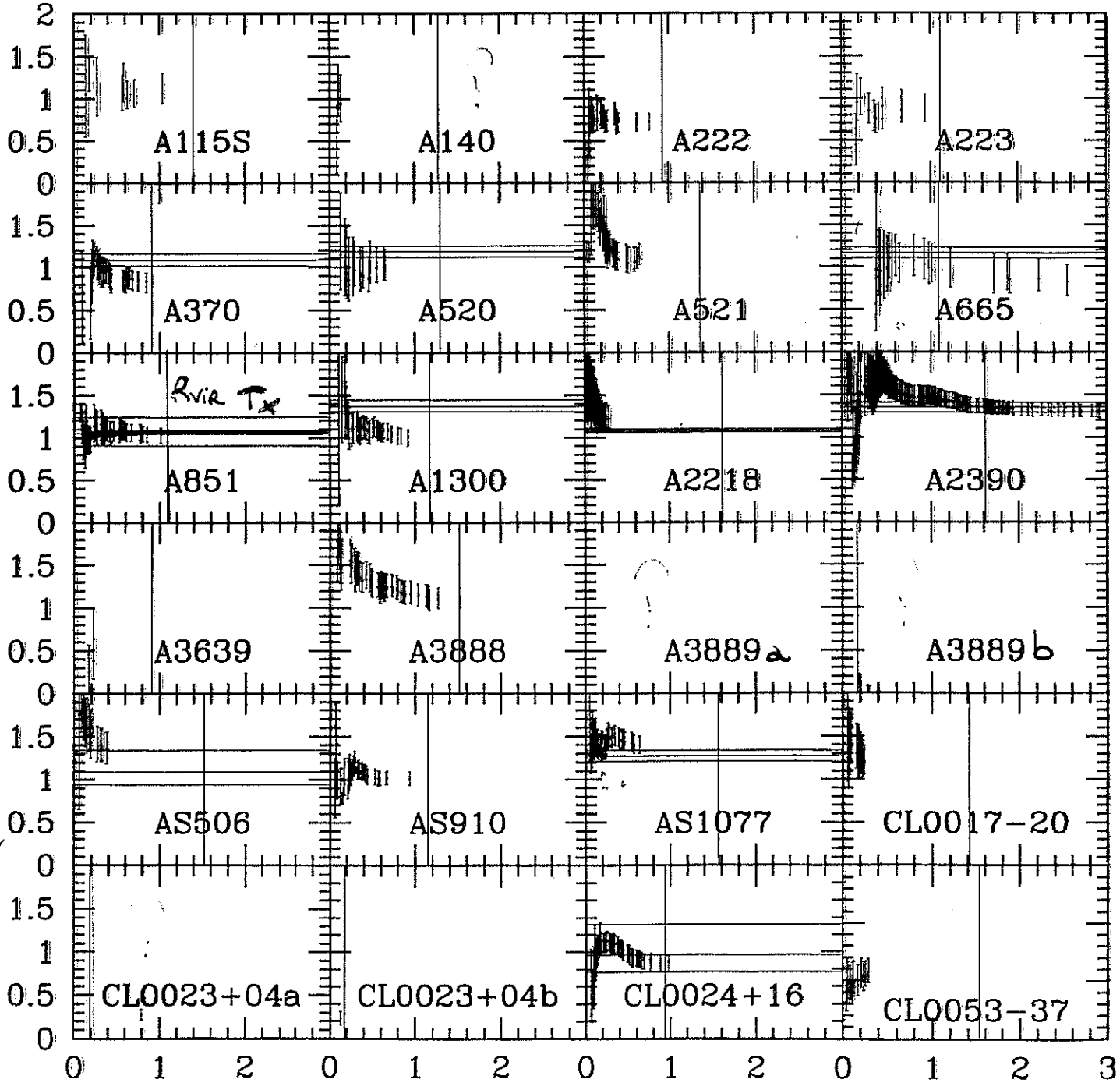

profili di dispersione "integrati" di velocità

OSSERVAZIONI

Velocity Dispersion Profiles and Velocity Anisotropies

(with Giuricin, Mardirossian, Mezzetti, and Boschin 1998, ApJ 505, 74)

Ensemble cluster built with gals of 160 nearby clusters⇒observational profile

Jeans eq.+ mass distribution+assumption for v–anisotropy⇒theoretical profile.

Mass–follows–light assumption

Velocity anisotropy parameter $\beta(\mathbf{r})=1-\sigma_\tau^2(\mathbf{r})/\sigma_r^2(\mathbf{r})=0$:

χ^2 goodness of fit is 96%.

The "average" cluster has isotropic velocities!

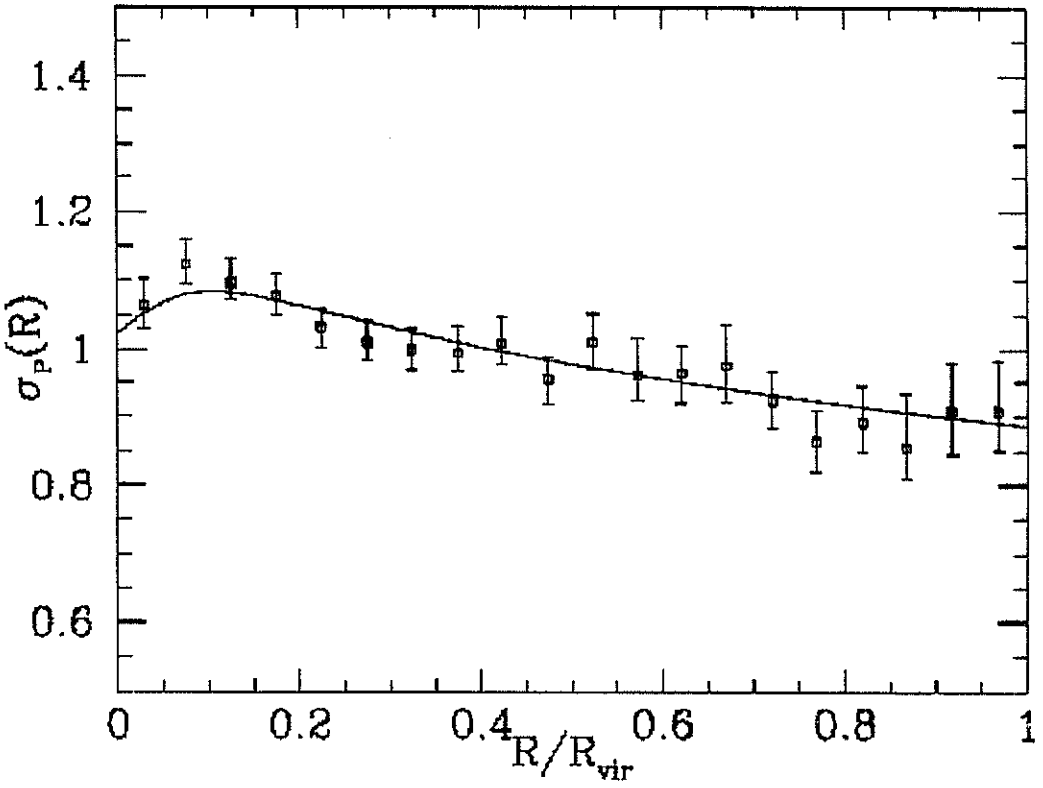

⇒Mean surface term correction to virial mass about 20%.

Profili di dispersione di velocità differenziali TEORIA CFR. DATI

Velocity Dispersion Profiles and Velocity Anisotropies

(coll. with Giuricin, Mardirossian, Mezzetti, and Boschin 1998, ApJ 505, 74)

3 families of clusters (for $\neq \sigma_v$ in central regions/σ_{TOT})⇒3 ensemble clusters.

Jeans eq.+ mass distribution+assumption for anisotropy⇒theoretical profile

$M \propto L$

$$\beta(r) = 1 - \sigma_\tau^2(r)/\sigma_r^2(r)$$

Radial orbits in external regions (infall of galaxies?);
isotropic orbits (violent relaxation?);
circular orbits in internal regions (secondary relaxation phenomena?).

⇒Surface term correction to virial mass about 20–40%.

Clusters may be characterized by different anisotropies...
different stages of evolution?

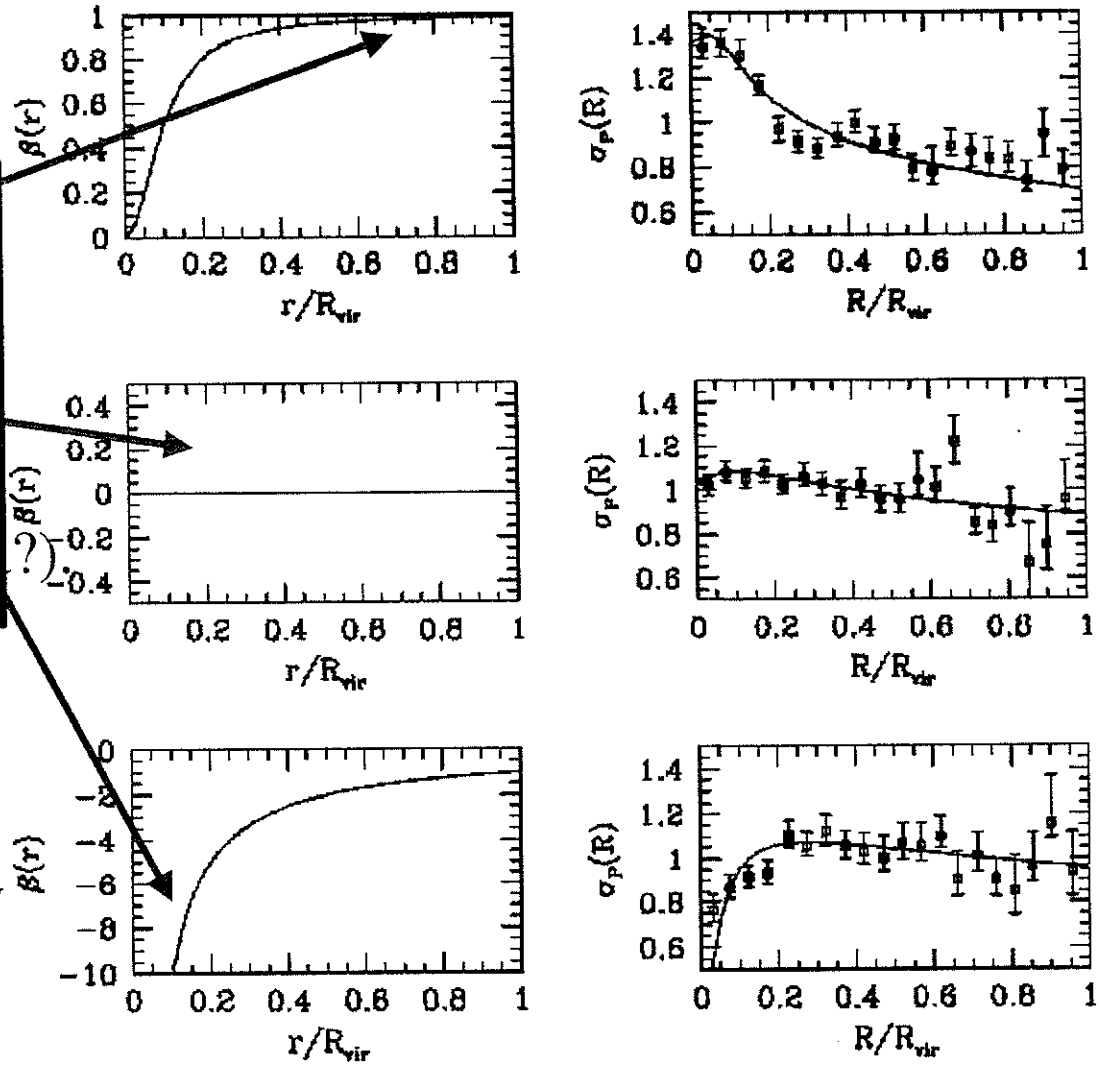

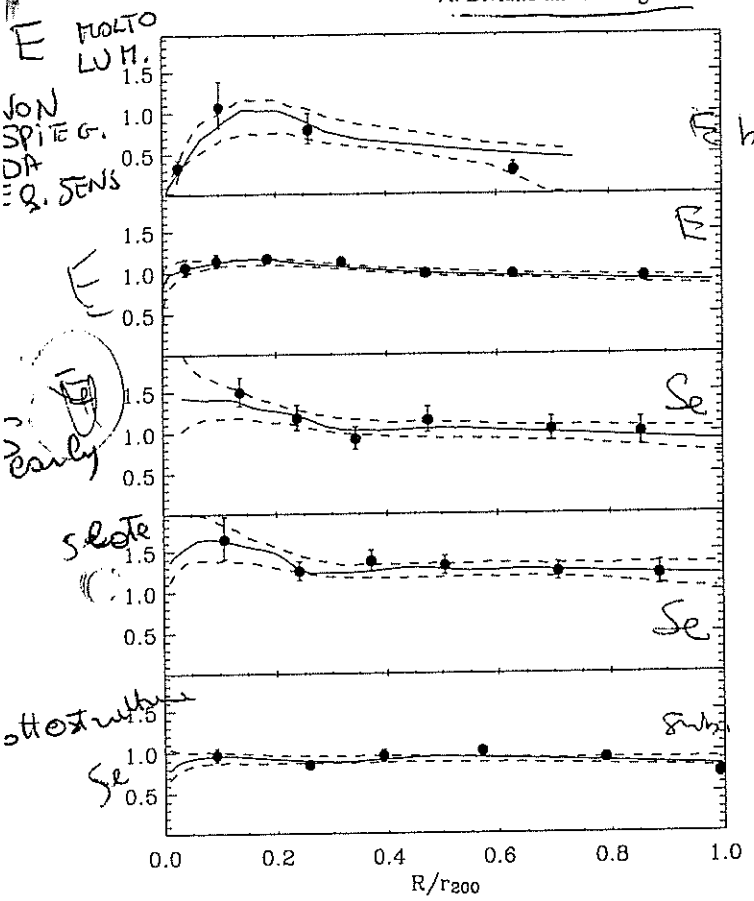

Fig. 2. The best LOWESS estimate (heavy line) of $\sigma_p(R)$, together with the 68% confidence levels (dashed lines), for each of the 5 galaxy classes, *from top to bottom*: E_{br}, Early, S_e, S_l, Subs. The filled circles with error bars indicate binned biweight estimates of $\sigma_p(R)$. The scale on the y-axis is in units of the global cluster velocity dispersion, calculated for all galaxies irrespective of type.

To our knowledge, this is the first time that the number-density and velocity-dispersion profiles for these 5 cluster galaxy classes have been derived with such accuracy and in such detail. Therefore, we briefly comment on the qualitative nature of the different $I(R)$, $\nu(r)$ and $\sigma_p(R)$ before proceeding with the analysis.

Among galaxies outside substructure, the E_{br} have the steepest density profile in the centre, followed by the Early, the S_e, and the S_l. This is a clear manifestation of the morphology-density relation (e.g. Dressler 1980), and of luminosity segregation (e.g. Rood & Turnrose 1968 and Paper XI). Interestingly, the density profiles of both S_e and S_l decrease towards the cluster centre, a clear indication that these galaxies avoid the central cluster regions. On the contrary, E_{br} are mostly found in the central cluster regions.

The Subs galaxies have a number-density profile that is rather steep in the centre, but shows a weak "plateau" at $\sim 0.6\, r_{200}$. Note that the number density profile of this galaxy class could, in principle, be biased by systematic effects due to the selection procedure of the members of substructures, which might result in a radius-dependent detection efficiency. A comparison of the de-projected number densities of the Subs-class galaxies and of the bulk of the galaxies outside substructures, viz. the Early-class galaxies (right-hand panels of Fig. 1), shows that, within $\sim 0.6\, r_{200}$, the two profiles have essentially identical logarithmic slopes. Beyond $\sim 0.6\, r_{200}$ the number-density profile of the Subs galaxies is quite a bit flatter than that of the Early galaxies, until it steepens again beyond $\sim 1.0\, r_{200}$. This was already noted in Paper XI. A comparison of the number-density profile of the Subs galaxies with that obtained by De Lucia et al. (2004) from their numerical models of substructures in cold dark matter haloes gives a similar result. The logarithmic slope between $0.1\, r_{200}$ and $0.8\, r_{200}$ of the number-density of haloes with masses $\sim 10^{13}\, M_\odot$ is about -1.6, not very different from that of the Subs galaxies which is -1.5.

The velocity dispersion of the E_{br} strongly decreases towards the centre, with a slower but equally large decrease outwards (remember that *all* velocity dispersions are normalized by the same, global velocity dispersion calculated for *all* galaxies irrespective of type). The special formation history and location of the E_{br} at the bottom of the cluster potential well is reflected in their very low central velocity dispersion. In contrast, galaxies of the Early class have a rather flat velocity-dispersion profile, changing by only $\approx \pm 20\%$ over the virial region. The velocity-dispersion profiles of S_e and S_l are rather similar, starting at high values near the centre with a fairly rapid decrease out to $r \approx 0.3\, r_{200}$, and flattening towards larger projected distances. Yet, the velocity dispersion of the S_l is larger than that of the S_e (and, in fact, of any other class) at all radii. It is perhaps interesting to note that the velocity-dispersion profiles of S_e and S_l are remarkably similar to those of, respectively, the "backsplash" and infalling populations of subhaloes found in the numerical simulations of Gill et al. (2004).

Finally, the velocity-dispersion profile of the Subs class is very "cold" and flat, even flatter and "colder" than that of the Early class. One might wonder if this is due to the procedure by which the galaxies of the Subs class were selected, but it is very unlikely that the velocity dispersion of the Subs class is biased low by the selection. If anything, the actual velocity dispersion of the subclusters is overestimated because the internal velocity dispersion of the subclusters has not been corrected for. In Sect. 6.4 we discuss several estimates for the real velocity-dispersion profile, i.e. corrected for internal velocity dispersion and possible bias due to the selection.

4. The mass profile

In addition to the observed $I(R)$-, $\nu(r)$- and $\sigma_p(R)$-profiles presented in Sect. 3 we also need an estimate of the mass profile $M(<r)$ for a determination of the $\beta(r)$-profiles. The mass profile that we will use here is the one that was derived in Paper XII, from the number density and velocity-dispersion profiles of the Early-class galaxies. As discussed in detail in Paper XII, the Early-class galaxies are likely to be in equilibrium with the cluster potential, as the formation of most of them probably antedates their entry into the cluster, so that they have had ample time to settle in the potential. In Paper XII we also showed that galaxies of the Early class have a nearly isotropic velocity distribution; this follows from an analysis of the shape of the distribution of their line-of-sight velocities. More specifically, assuming a constant velocity anisotropy for the

N(v) ⇒ ORBITE
MOMENTI SUCCESSIVI ALL'EQ. DI JEANS

distribution as a function of projected radius. In effect, this technique would require any model of Coma to be consistent not only with the Jeans equation, but also with the more detailed Boltzmann equation from which the Jeans equation is derived. No one has yet described the best way to carry out this task (nor is there any cluster that is both sufficiently well observed, and convincingly close to equilibrium, to justify such an analysis). In the case of Coma, one way to make use of the extra information contained within the full velocity distribution function is illustrated in Figure 2. The overall velocity histogram appears marginally most consistent with a high–mass, radial–orbit model; a model with low mass and circular orbits appears strongly inconsistent. There are, however, a number of reasons to be cautious about this comparison. The shape of the velocity histogram can be strongly affected by processes such

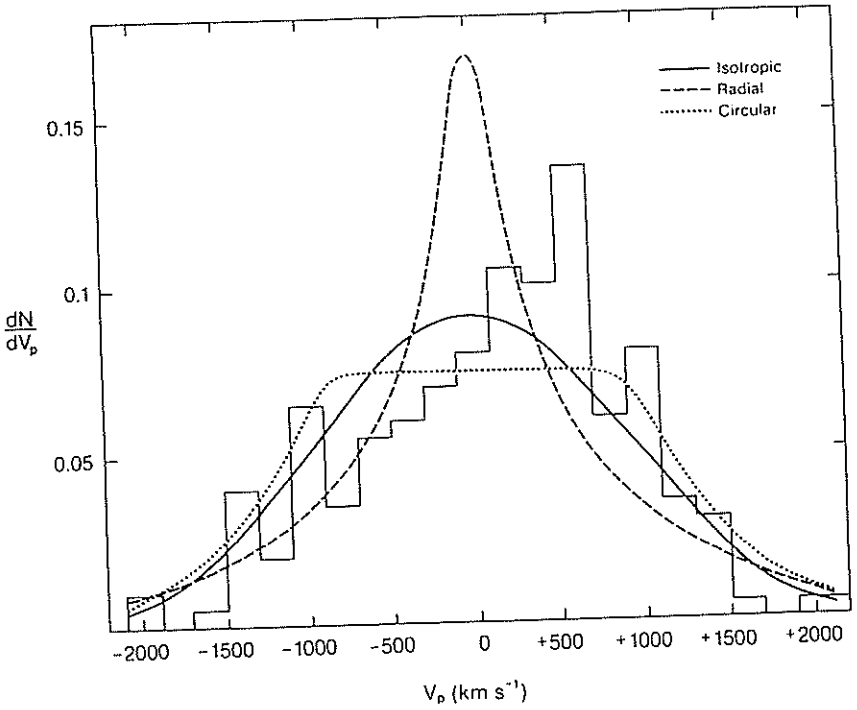

Fig. 2 Velocity histogram for galaxies in Coma. The three curves are derived from models in which the galaxy orbits are isotropic, radial, and circular; the dark matter distributions have been adjusted to give the same line–of–sight velocity dispersion profile in each case. (From Merritt, *Ap. J.*, **313**, 121.)

as rotation and infall which we have so far neglected. In fact, inspection of Figure 2 reveals a possibly significant ($\sim 97\%$ confidence) degree of skewness in the observed distribution. Cluster rotation by itself would tend to broaden

not exhibit significant rotation (Rood et al. 1972). However there is good reason to believe that contamination by foreground galaxies might explain the low–velocity "tail". De Lapparent, Geller and Huchra (1986) show that the Coma cluster appears to sit at the intersection of a number of large–scale galaxy "shells", one of which lies nearly along the line of sight to Coma. These foreground galaxies could significantly affect the form of the overall velocity histogram, even if they have little effect on the inferred dynamics of the central regions.

A number of other techniques have been discussed for constraining the orbital kinematics of galaxies in clusters. Pryor and Geller (1984) attempted to use the observed tidal radii and gas content of galaxies in Coma to put limits on their orbital pericenters, and hence on the degree of velocity anisotropy. Their result (that the Coma cluster is close to isotropic within $1h^{-1}$ Mpc) is strongly dependent on the uncertain physics of tidal truncation and gas dynamical ablation; furthermore those authors only considered models in which the dark matter is distributed like the galaxies, while in fact the available velocity data imply a fairly tight relation between the mass distribution and the galaxy orbits, as discussed above. O'Dea, Sarazin and Owen (1987) used the orientation of "narrow angle tail" radio sources in clusters to constrain the distribution of galaxy orbits, under the assumption that the radio–luminous plasma ejected by a moving galaxy is bent into a tail which marks the path taken by the galaxy through the cluster. Since most clusters contain only a few such radio sources (Coma, for instance, contains only one), those authors were forced to superpose data from many clusters. They obtained the surprising result that galaxy orbits in the inner $\sim 0.5h^{-1}$ Mpc of their clusters are strongly *radial*; at large radii the distribution of tail orientations appears to be random. The correct interpretation of this result will probably have to await a better understanding of the gas ablation process. It may be, for instance, that the probability of observing a galaxy as a narrow angle tail depends strongly on its velocity with respect to the intracluster gas, in which case the observed sample could be kinematically biased.

For a long time it was hoped that X–ray observations of hot intracluster gas would resolve the indeterminacy of cluster masses. The equation of hydrostatic equilibrium, in spherical symmetry, states

$$\frac{d\Phi}{dr} = \frac{GM(r)}{r^2} = -\frac{1}{\rho_g}\frac{dP_g}{dr} = -\frac{1}{\rho_g}\frac{d}{dr}\left(\rho_g k T_g\right), \qquad (10)$$

where ρ_g and T_g are the gas density and temperature. Equation (10) is simpler than the Jeans equation (3) since gas is a collisional fluid with an isotropic pressure; thus the two functions $\{\sigma_r(r), \sigma_t(r)\}$ are replaced by one, $T_g(r)$. Furthermore, the statistical accuracy of a mass determination based on the X–ray emitting gas can always be increased by lengthening the integration time, whereas the number of bright galaxies in a cluster is limited. Unfortunately, the spatial resolution of the spectral instruments on past X–ray satellites has not been very good, and at present there is no cluster (with the possible exception of Virgo) for which we have an accurate determination of $T_g(r)$. This problem is capable of solution; future satellites, such as AXAF, should yield accurate temperature profiles and hence accurate masses for nearby clusters. However

TEOREMA DEL VIRIALE
GENERALIZZATO

E PROBLEMA

MASS FOLLOWS LIGHT ?

(Sì !)

Teorema del viriale "generalizzato"
(es. Merritt 1988 Minnesota Lectures)

$m = \nu$

$$m\frac{d\phi}{dr} = \frac{mGM(r)}{r^2} = -\frac{d(m\sigma_r^2)}{dr} - \frac{2m}{r}\left(\sigma_r^2 - \sigma_\theta^2\right)$$

$\times 4\pi r^3$ e $\int_0^\infty dr$

$$\int_0^\infty m\frac{d\phi}{dr}\,4\pi r^3 dr = \int_0^\infty -\frac{d(m\sigma_r^2)}{dr}\,4\pi r^3 dr - \int_0^\infty \frac{2m}{r}\left(\sigma_r^2-\sigma_\theta^2\right)4\pi r^2 dr$$

$$= -\left| m\sigma_r^2\,4\pi r^3 \right|_0^\infty + \int_0^\infty m\sigma_r^2\,12\pi r^2 dr - \int_0^\infty 2m\left(\sigma_r^2-\sigma_\theta^2\right)4\pi r^2 dr$$

$= 0$ perché $r(0)=0$, $\sigma(\infty)=0$

$$= \int_0^\infty 4\pi r^2 m\underbrace{\left(-2\sigma_r^2 + 2\sigma_\theta^2 + 3\sigma_r^2\right)}_{\underbrace{2\sigma_\theta^2+\sigma_r^2}_{\sigma^2}} dr$$

$$\frac{\int_0^\infty r\frac{d\phi}{dr}\,m\,4\pi r^2 dr}{\int_0^\infty m\,4\pi r^2 dr} = \frac{\int_0^\infty \sigma^2 m\,4\pi r^2 dr}{\int_0^\infty m\,4\pi r^2 dr}$$

← aggiungo /...

cioè $\left\langle r\frac{d\phi}{dr}\right\rangle = \langle\sigma^2\rangle$ medie spaziali

Teorema del Viriale generalizzato (ct.)

$$\left\langle r \frac{d\phi}{dr} \right\rangle = \langle \sigma^2 \rangle$$

$$\frac{d\phi}{dr} = \frac{GM(r)}{r^2} = \frac{GM_\infty F(r)}{r^2} \qquad \text{dove } F(r) \equiv \frac{M(r)}{M_\infty} \leq 1$$

$$\left\langle r \frac{d\phi}{dr} \right\rangle = \left\langle \frac{GM_\infty F(r)}{r} \right\rangle = \langle \sigma^2 \rangle$$

$$GM_\infty = \frac{\langle \sigma^2 \rangle}{\langle r^{-1} F \rangle}$$ Teorema del Viriale

Non dipende da β anisotropia di velocità $\langle \sigma^2 \rangle = 3 \langle \sigma^2_{los} \rangle$

MA... devo avere ipotesi su $F(r)$

SE $F(r) \propto M(r)$ (MASS FOLLOWS LIGHT ASSUMPTION !)

$$GM_\infty = \frac{3\pi}{2} \frac{\langle \sigma^2_{los} \rangle}{\langle r_{ij}^{-1} \rangle_{solo\ i>j}} = \frac{3\pi}{2} \langle \sigma^2_{los} \rangle R_{VT}$$

Lynden Bell 67

$$R_{VT} = \frac{1}{\langle r_{ij}^{-1} \rangle_{solo\ i>j}} = 2 R_H = \frac{2 \frac{N(N-1)}{2}}{\sum_{ij} R_{ij}^{-1}}$$

raggio del Teorema del Viriale

raggio armonico

$\frac{\pi}{2}$ = fattore di proiezione per i raggi

3 = fattore di proiezione di $\sigma^2_{1D \to 3D}$

$$M_\infty = \frac{3\pi}{2} \frac{\sigma^2_{los} R_{VT}}{G}$$ (= Teorema del Viriale × N punti massa, Vedi corso Mandrossian)

M CFR L M/L=cost VERO? SI!

INFORMATION ON DM FROM CLUSTERS

The amount of DM

Zwicky (1933): large amount of DM in Coma cluster; baryon fraction $M_b/M_{CLUSTER} \gtrsim 5\% h^{-3/2}$ $h = H_0/(100 km/s\ Mpc^{-1})$ (e.g. White et al. 1993; White & Fabian 1995; David, Jones, & Forman 1996; Cirimele, Nesci, & Trevese 1997)

if cluster baryon fraction is representative of the Universe $\Omega_b/\Omega_0 \gtrsim 0.05 h^{-3/2}$ must be compared with $\Omega_b \sim 0.01, < 0.025 h^{-2}$ predicted by cosmic (standard) nucleosynthesis $\Rightarrow \Omega_0 < 1$ (e.g. Evrard 1996)

BUT $M_{CLUSTER}$ =?... disagreement (for a factor of 2-3) between masses obtained with different methods (e.g. Miralda et al. 1993; Wu & Fang 1997)

The shape of DM distribution

DM distribution is less extended than gas distribution and (maybe?) follows galaxy number distribution with a more peaked concentration in central cluster regions (e.g. Watt et al. 1992; Mushotzky 1992; Durret et al. 1994; Narayan & Bartelmann 1997)

Carlberg et al 97

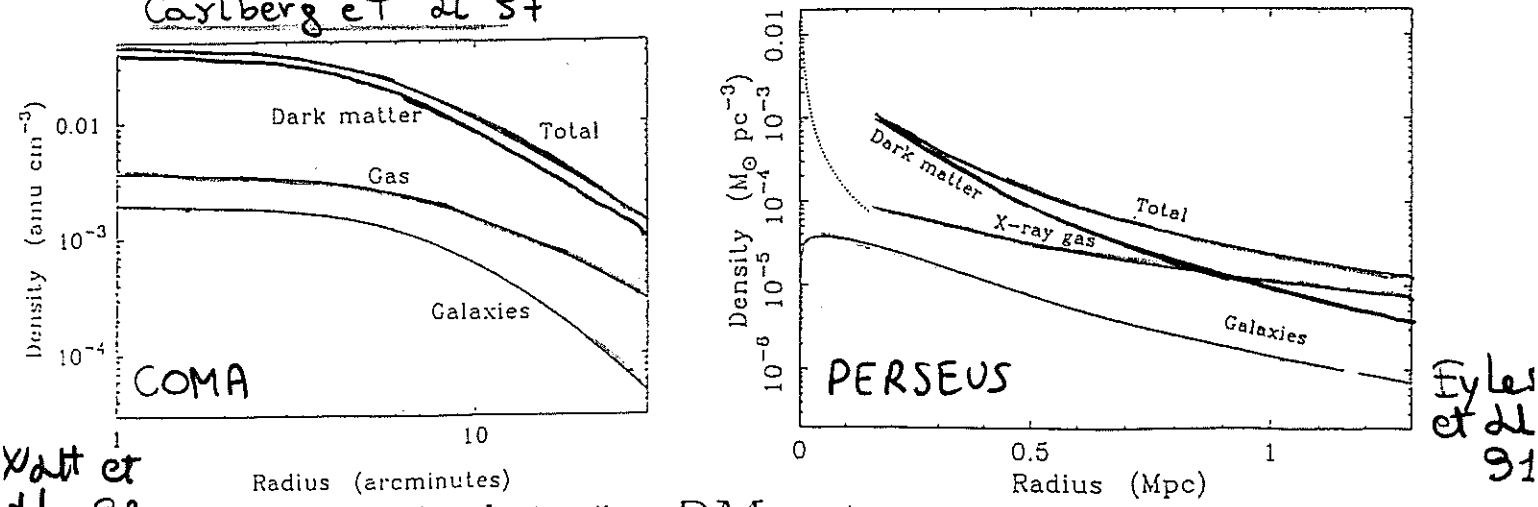

Watt et al. 92

Eyles et al 91

$\Rightarrow$ constraints for DM nature (e.g. Eyles et al. 1991)

Constraints for DM cosmological scenarios derived from the observational distribution of abundances of clusters as a function of their mass (or velocity dispersion

M SEGUE L

Mass and Light Distribution

From gravitational lensing: **mass distribution and galaxy light distribution look similar**, with roughly the same orientation and ellipticity.

Two dark matter clumps in sentral regions of A2218 **(Kneib, Mellier, Pelló et al. (1995)**.
Left panel: crossed circles represent galaxies;
right panel: iso-mass contours derived from the lensing model.

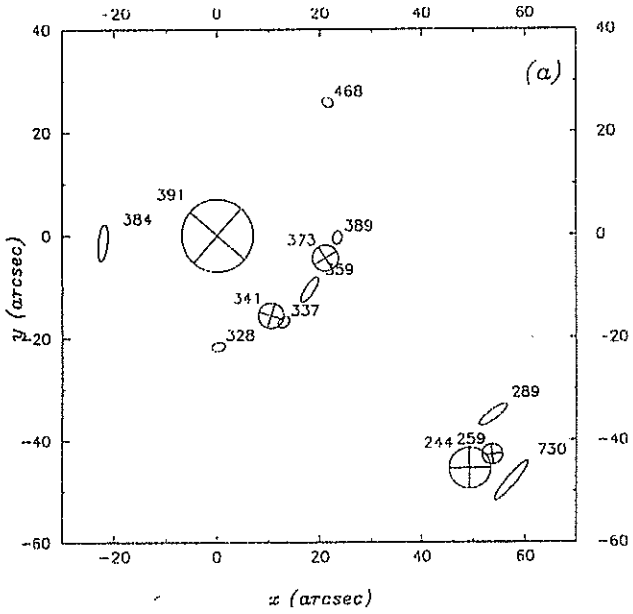

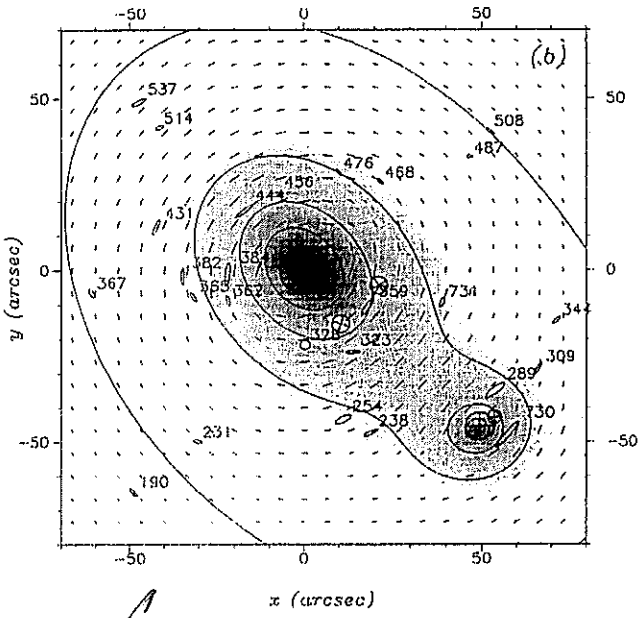

TOTAL MASS

Mass Comparison: the case of MS 1008−1224 at z~0.3

(Lombardi, Rosati, Nonino, MG, Borgani Squires 2000, A&A 363, 401)

Mass from:
ICM (ROSAT data);
galaxy kinematics (CNOC data);
weak lensing (VLT data).

OK global estimate.
Central region?

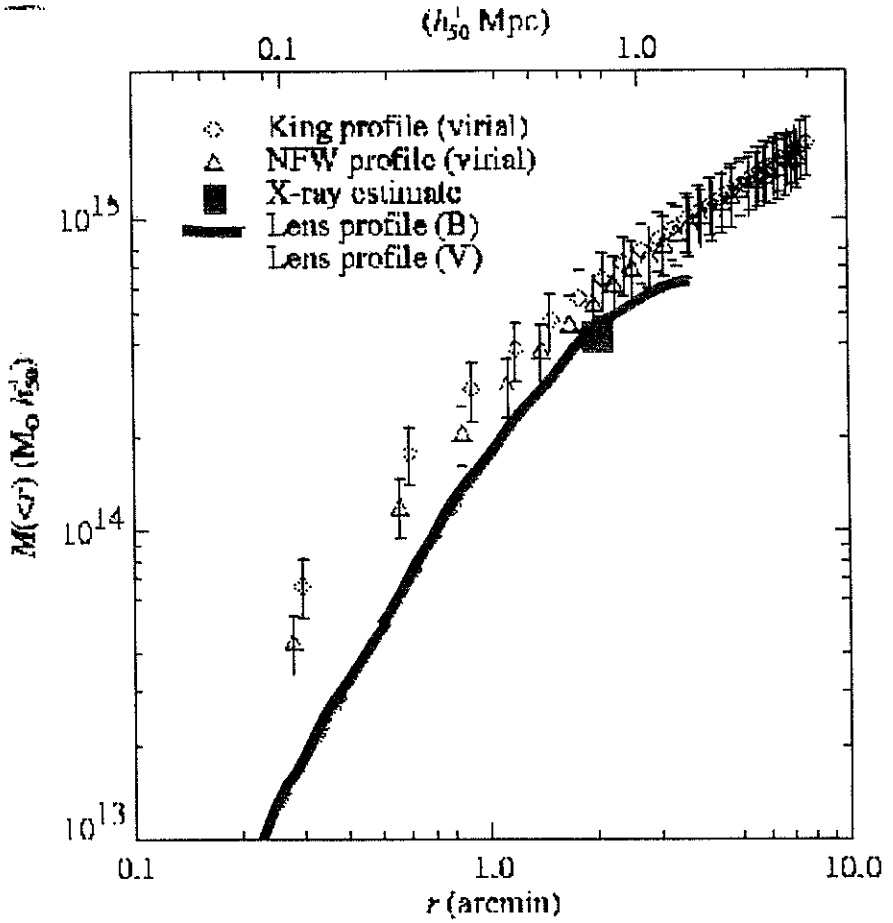

Mass Comparison

IPOT. DI EQUILIBRIO DINAMICO

M_X vs. M_{opt} (Girardi et al. 1998; Lewis et al. 1999)

↳ + IPOTESI M SEGUE L

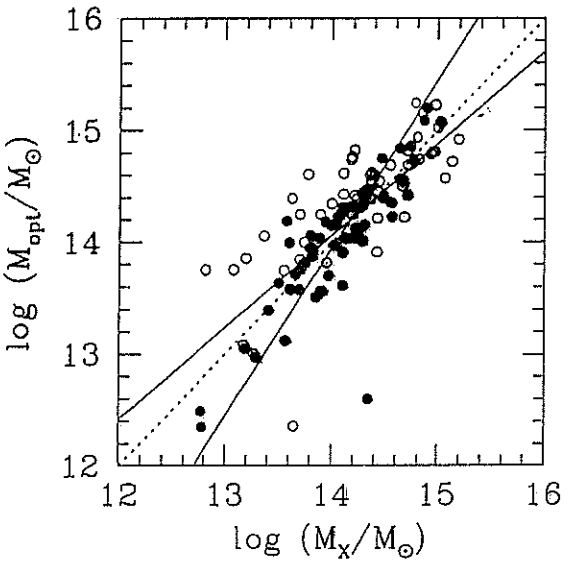

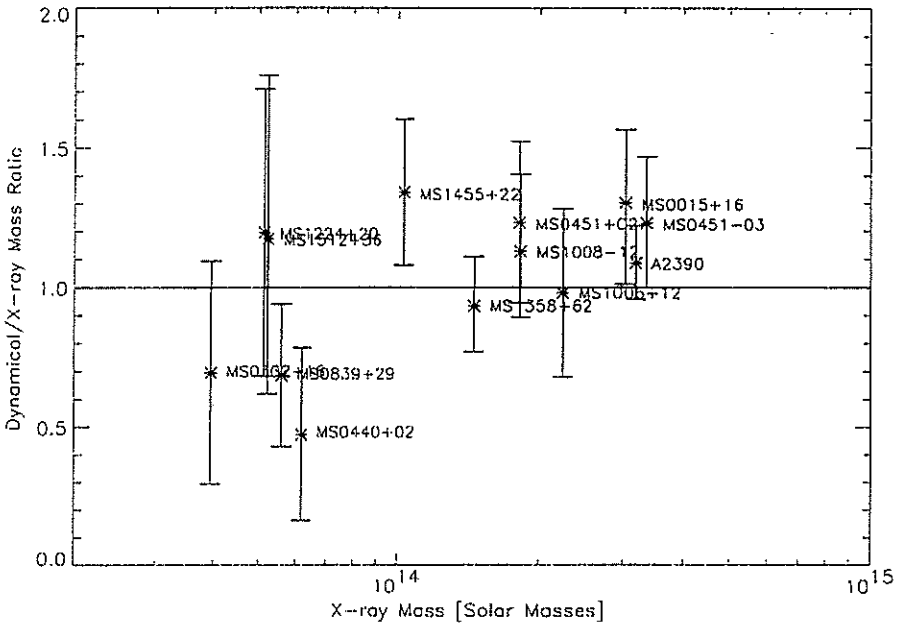

From **Allen (1998)** M_{lens} vs. M_X (strong lensing):

NON RICHIEDE IPOTESI DI EQUILIBRIO DINAMICO

circles: cooling-flow clusters,
squares: no cooling clusters,
pinched squares: intermediate.

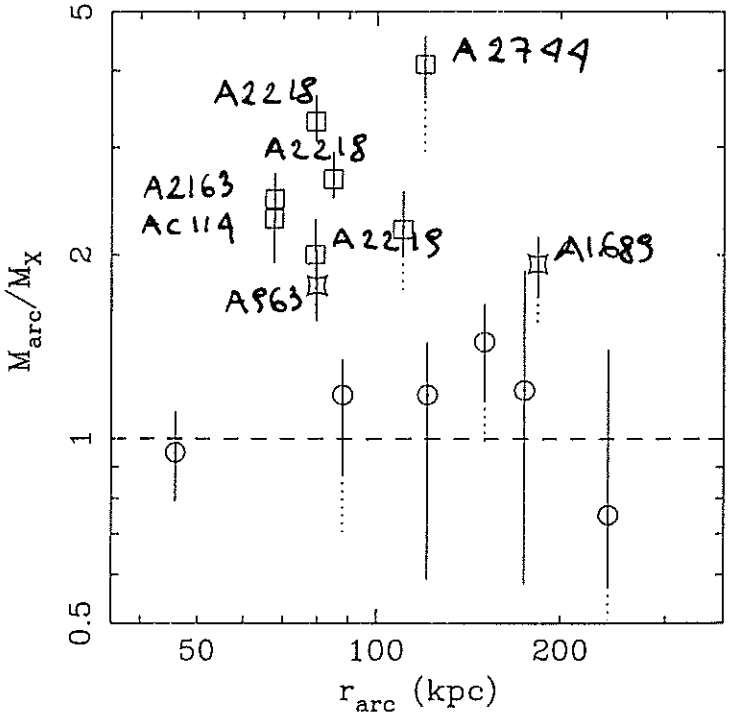

MASSA DAL GRAVITATIONAL LENSING

già Zwicky 1937 aveva intuito la possibilità che ammassi di galassie si comportassero da lenti.

La prima volta che si vede un arco: A370 (Fort et al 86)

PRINCIPI BASE:

una massa cambia la posizione apparente di una sorgente $\vec{\theta}_s$ in quella dell'immagine $\vec{\theta}_i$ di una quantità $\vec{\alpha}$ $\quad \vec{\theta}_s = \vec{\theta}_i + \vec{\alpha}(\vec{\theta}_i)$

dove $\vec{\alpha} = \vec{\nabla}\phi_{2D}$ (potenziale proiettato)

L'amplificazione e distorsione degli oggetti di fondo sono descritti dalla matrice A (di amplificazione) che il piano sorgente ed il piano immagine $\vec{\theta}_s = \begin{pmatrix} 1-K-\gamma & 0 \\ 0 & 1-K+\gamma \end{pmatrix} \vec{\theta}_i$

dove K = convergenza e γ = deformazione di taglio

$K = \frac{1}{2}\nabla^2\phi_{2D} = \frac{\Sigma}{\Sigma_{crit}} = l$ = densità di massa proiettata

Strong lensing $l >> 1$ e a $K \sim 1$ (archi e archetti)

CASO PARTICOLARE

arco gigante di Einstein con S allineata con L

Cerchio di raggio ξ_{crit}

$\frac{M(<\xi_{crit})}{\pi \xi_{crit}^2} = \Sigma_{crit} = \frac{c^2}{4\pi G}\frac{D_{OS}}{D_{OL}D_{SL}}$

dove sappiamo z_S, ma dipende poco da H_0 e Ω

CFR. MASSA DA JEANS
TE DA VIRIALE

CORRETTIONE DEL TERMINE
DI PRESSIONE SUPERFICIALE
(DOVUTO A $\sigma_z(R_{MAX}) \neq 0$)

RED / BLUE GALAXIES

CNOC CLUSTERS

CARLBERG ET AL. 1997

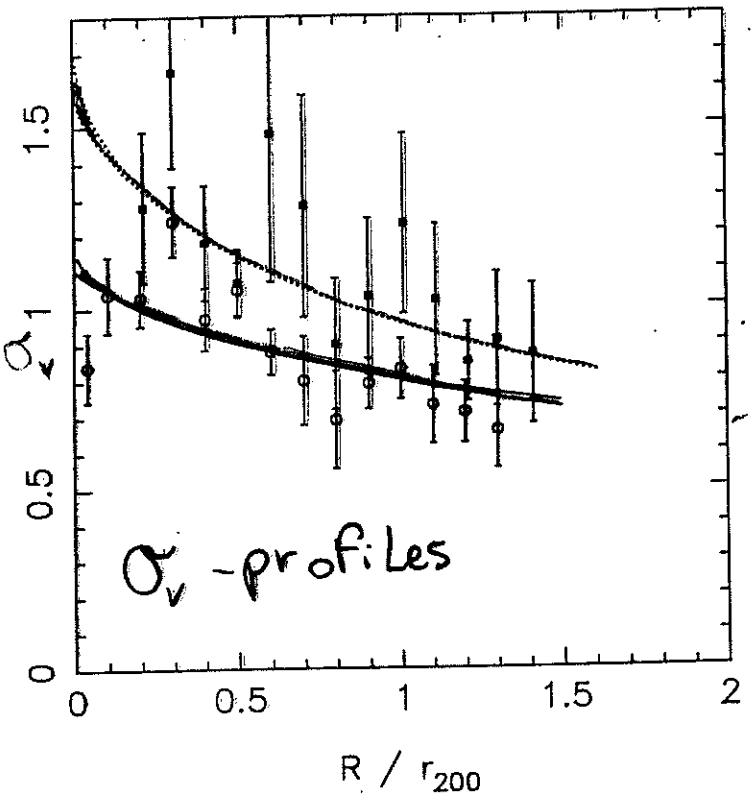

density profiles

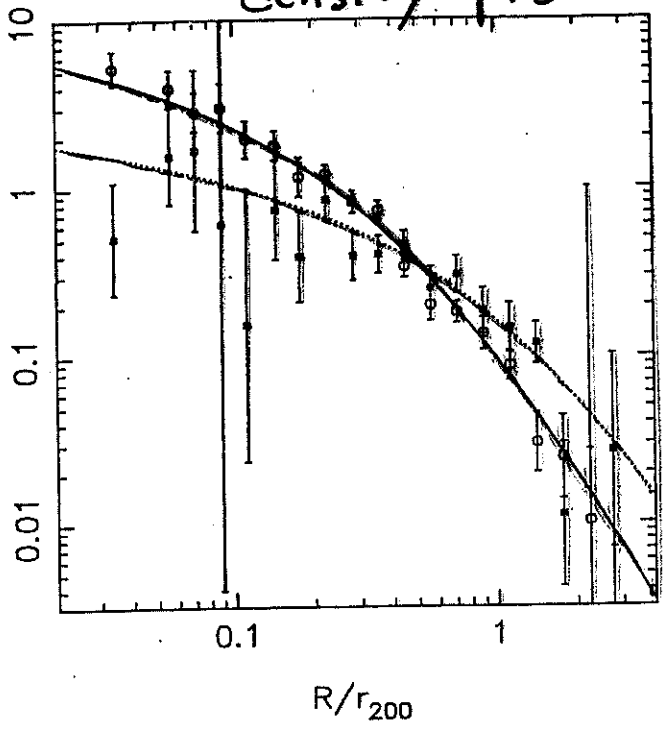

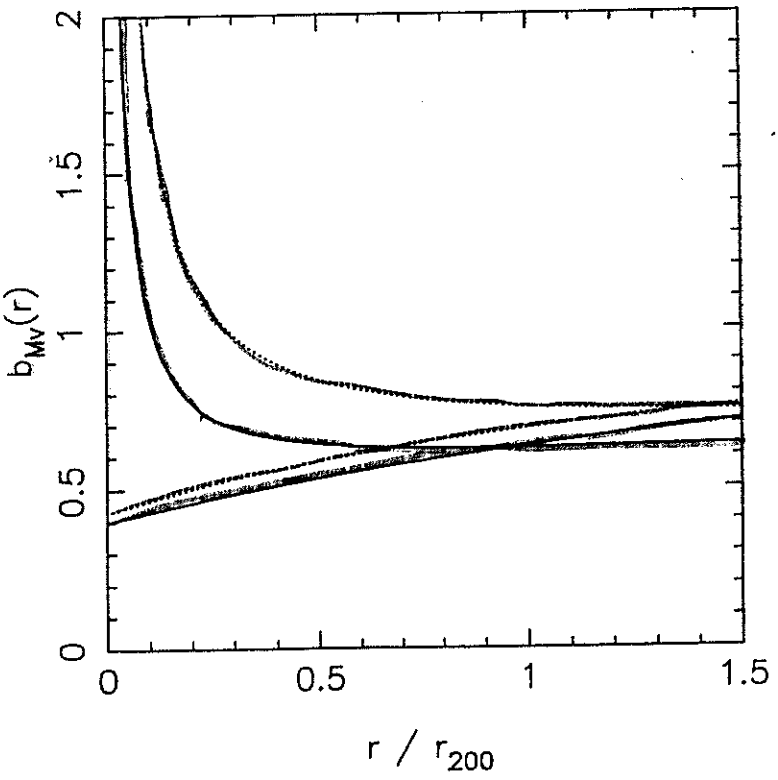

$\left(\frac{M_{JEANS}}{L(r)} \cdot \frac{\tilde{L}}{\tilde{M}_{VIR}}\right)$ → DIFFERENZA DA 1 È LA PRESSURE TERM CORRECTION (~20%)

$M_{VIR}^{BLUE} \sim 3\, M_{VIR}^{RED}$

BUT

JENS eq. ⇒ blue galaxies and red galaxies in equilibrium within the same potential

Virial vs. Jeans Mass Estimates

Jeans equation+ flat σ_v–profile

+isotropic orbits

$\Rightarrow \mathbf{M_{iso}(<r)=3\beta_{fit,gal}\sigma_v^2 r/G}$

Median value from the fits: $\beta_{fit,gal}$=0.8.

M_{iso}(<Rvir).

Virial mass.

Virial mass with surface term correction.

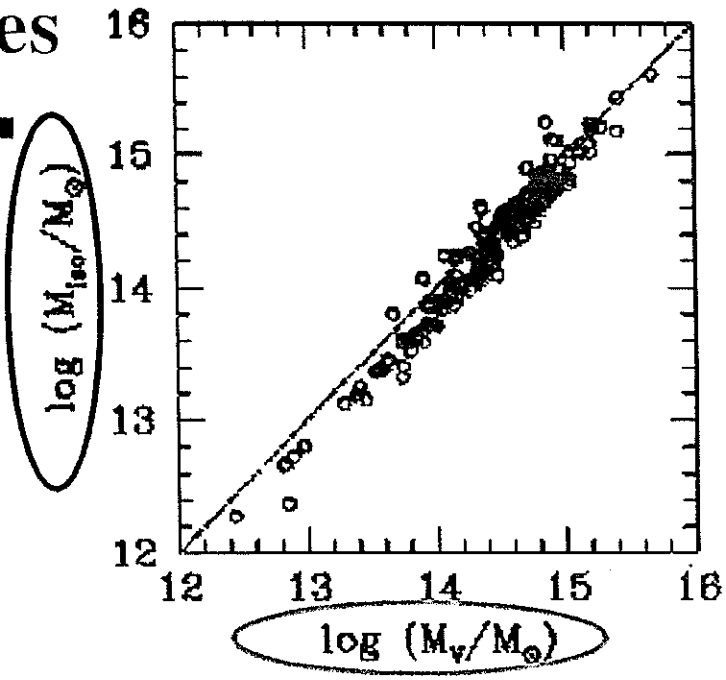

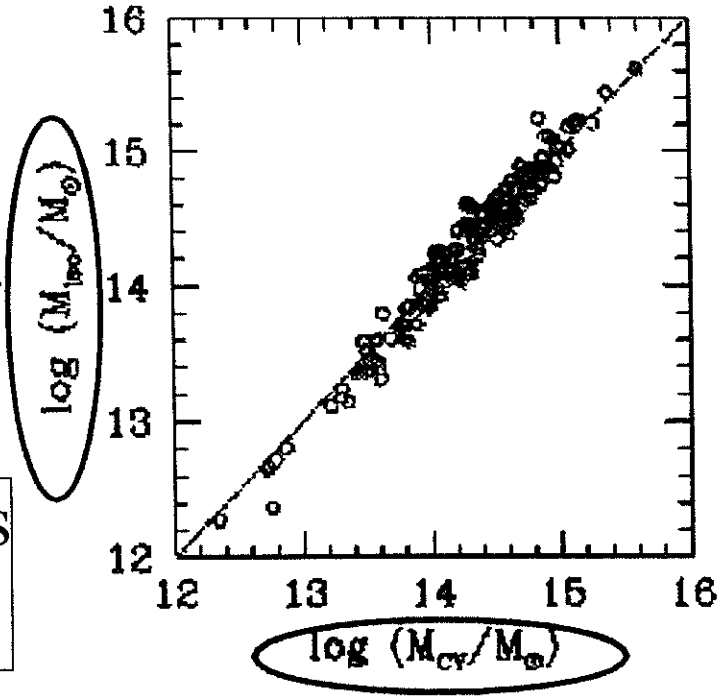

M_{iso}(<Rvir) ~Corrected virial mass

⇒Selfconsistency verification.

Teorema del viriale:
Termine di correzione di pressione superficiale
es. Binney-Tremaine / Girardi et al 98, The and ref G 96
(Carlberg et al 96-98) SPT

$$n\frac{d\phi}{dr} = n\frac{GM(r)}{r^2} = -\frac{d(n\sigma_r^2)}{dr} - \frac{2n}{r}\left(\sigma_r^2 - \sigma_\theta^2\right)$$

$$\times 4\pi r^3 \int_0^{r_{max}} \longrightarrow \text{raggio max delle osservazioni}$$

a sinistra:

$$\int_0^{r_{max}} n\frac{d\phi}{dr}\, 4\pi r^3 dr = \left\langle r\frac{d\phi}{dr}\right\rangle_{r_{max}} \cdot \int_0^{r_{max}} n\, 4\pi r^2 dr$$

a destra

$$-\left| n\sigma_r^2 4\pi r^3 \right|_0^{r_{max}} + \underbrace{\int_0^{r_{max}} 4\pi r^2 n\sigma_r^2 dr - \int_0^{r_{max}} 4\pi r^2 n\left(-2\frac{\sigma_r^2}{r}+2\frac{\sigma_\theta^2}{r}\right)dr}$$

$\hookrightarrow \sigma(r_{max}) \neq 0$!

$$\int_0^{r_{max}} 4\pi r^2 n\sigma^2 dr$$

$$-n\sigma_r^2(r_{max})4\pi r_{max}^3 + \langle\sigma^2\rangle_{r_{max}} \int_0^{r_{max}} n\,4\pi r^2 dr$$

$$\left\langle r\frac{d\phi}{dr}\right\rangle_{r_{max}} = \frac{-n\sigma_r^2(r_{max})\,4\pi r_{max}^3}{\int_0^{r_{max}} n\,4\pi r^2 dr} + \langle\sigma^2\rangle_{r_{max}}$$

$$\left\langle r\frac{GM(r_{max})F(r)}{r^2}\right\rangle_{r_{max}} = GM(r_{max})\langle r^{-1}F(r)\rangle_{r_{max}}$$

$$M(r_{max}) = \frac{\langle\sigma^2\rangle_{r_{max}}}{G\langle r^{-1}F\rangle_{r_{max}}} - \frac{n\sigma_r^2(r_{max})4\pi r_{max}^3}{G\langle r^{-1}F\rangle_{r_{max}}\int_0^{r_{max}} 4\pi r^2 n\, dr}$$

$\hookrightarrow$ M viriale standard

$$M(r_{max}) = M_{VSTAND}\left(1 - \underbrace{\frac{4\pi r_{max}^3 n(r_{max})}{\int_0^{r_{max}} 4\pi r^2 n\, dr}}_{\text{dipende da profilo di struttura}} \cdot \underbrace{\frac{\sigma_r^2(r_{max})}{\langle\sigma^2\rangle_{r_{max}}}}_{\text{dip. da anisotropia vel. se è isotropo } 1/3}\right) \longrightarrow \text{osserv.}$$

Tipicamente
Corr. = 20% di $M_{VstandAd}$ $\times R_{max} = R_{200}$

X SURFACE PRESSURE CORRECTION E ANISOTROPIE DI VELOCITÀ

THE ASTROPHYSICAL JOURNAL, 505:74–95, 1998 September 20
© 1998. The American Astronomical Society. All rights reserved. Printed in U.S.A.

OPTICAL MASS ESTIMATES OF GALAXY CLUSTERS

MARISA GIRARDI,[1,2,3] GIULIANO GIURICIN,[2,3] FABIO MARDIROSSIAN,[1,2,3] MARINO MEZZETTI,[2,3] AND WALTER BOSCHIN[2,3]
Received 1998 January 13; accepted 1998 April 22

ABSTRACT

We evaluate in a homogeneous way the optical masses of 170 nearby clusters ($z \lesssim 0.15$). The sample includes both data from the literature and the new ESO Nearby Abell Clusters Survey (ENACS) data. On the assumption that mass follows the galaxy distribution, we compute the mass of each cluster by applying the virial theorem to the member galaxies. We constrain the masses of very substructured clusters (about 10% of our clusters) between two limiting values. After appropriate rescaling to the X-ray radii, we compare our optical mass estimates to those derived from X-ray analyses, which we compiled from the literature (for 66 clusters). We find a good overall agreement. This agreement is expected in the framework of two common assumptions: that mass follows the galaxy distribution and that clusters are not far from a situation of dynamical equilibrium, with both gas and galaxies reflecting the same underlying mass distribution. We stress that our study strongly supports the reliability of present cluster mass estimates derived from X-ray analyses and/or (appropriate) optical analyses.

Subject headings: galaxies: clusters: general — galaxies: fundamental parameters — X-rays: galaxies

1. INTRODUCTION

A knowledge of the properties of galaxy clusters plays an important role in the study of large-scale structure formation. In particular, the observational distribution of the abundance of galaxy clusters as a function of their mass places a strong constraint on cosmological models (e.g., Bahcall & Cen 1993; Borgani et al. 1997; Gross et al. 1998; White, Efstathiou, & Frenk 1993a). Moreover, recent studies stress the need for reliable estimates of cluster masses in order to constrain the ratio of the baryonic to the total mass and the consequent value of Ω_0 (e.g., White & Frenk 1991; White et al. 1993b).

Indeed, estimating cluster masses is not an easy task, in spite of the various methods available. Applying the virial theorem to positions and velocities of cluster member galaxies is the oldest method of cluster mass determination (e.g., Zwicky 1933). More recent methods are based on the dynamical analysis of hot X-ray–emitting gas (e.g., Cowie, Henriksen, & Mushotzky 1987; Eyles et al. 1991) and on gravitational lensing of background galaxies (e.g., Grossman & Narayan 1989).

Mass estimates derived from the dynamical analysis of gas or member galaxies based on the Jeans equation or its derivations, such as the virial theorem, assume that clusters are systems in dynamical equilibrium (e.g., Binney & Tremaine 1987). This assumption is not strictly valid; in fact, although clusters are bound galaxy systems, they have collapsed very recently or are just now collapsing, as is suggested by the frequent presence of substructures (e.g., West 1994). However, some analyses suggest that the estimate of optical virial mass is robust against the presence of small substructures (Escalera et al. 1994; Girardi et al. 1997a; see also Bird 1995 for a partially different result), although it is affected by strong substructures (e.g., Pinkney et al. 1996). Similar results are found in studies based on numerical simulations (e.g., Schindler 1996a; Evrard, Metzler, & Navarro 1996; Roettiger, Burns, & Locken 1996) for X-ray masses estimated with the standard β-model approach (Cavaliere & Fusco-Femiano 1976), although some authors have claimed that there is a systematic mass underestimation (e.g., Bartelmann & Steinmetz 1996).

Dynamical analyses based on galaxies have the additional drawback that the mass distribution or (alternatively) the velocity anisotropy of galaxy orbits should be known a priori. Unfortunately, the two quantities cannot be disentangled in the analysis of the observed velocity dispersion profile, but only in the analysis of the whole velocity distribution, which, however, requires a large number of galaxies (on the order of several hundreds; e.g., Dejonghe 1987; Merritt 1988; Merritt & Gebhardt 1994). Without some information on the relative distribution of dark and galaxy components, the virial theorem places only order-of-magnitude constraints on the total mass (e.g., Merritt 1987). The usual approach is to apply the virial theorem assuming that mass is distributed as in the observed galaxies (e.g., Giuricin, Mardirossian, & Mezzetti 1982; Biviano et al. 1993). This assumption is supported by several pieces of evidence from both optical (e.g., Carlberg, Yee, & Ellingson 1997a) and X-ray data (e.g., Watt et al. 1992; Durret et al. 1994; Cirimele, Nesci, & Trevese 1997), as well as from gravitational lensing data, which, however, suggest a smaller core radius (e.g., Narayan & Bartelmann 1997).

The mass estimates derived from gravitational lensing phenomena are completely independent of the cluster dynamical status, but a good knowledge of cluster geometry is required in order to go from the projected mass to the cluster mass (e.g., Fort 1994). Moreover, strong lensing observations give values for the mass contained within very small cluster regions ($\lesssim 100$ kpc), and weak lensing observations are generally more reliable in providing the shape of the internal mass distribution rather than the amount of mass (e.g., Squires & Kaiser 1996).

Up to now, few studies have dealt with wide comparisons between mass estimates obtained by different methods for the same cluster. Wu & Fang (1996, 1997) found that masses derived from gravitational lensing analyses are higher than those derived from X-ray analyses by a factor of 2, but agree

[1] Osservatorio Astronomico di Trieste, Via Tiepolo 11, I-34131 Trieste, Italy.
[2] Scuola Internazionale Superiore di Studi Avanzati, via Beirut 4, I-34014 Trieste, Italy; girardi@sissa.it, giuricin@sissa.it, mardiros@sissa.it, mezzetti@sissa.it, boschin@newton.sissa.it.
[3] Dipartimento di Astronomia, Università degli Studi di Trieste, Trieste, Italy.

FORMAZIONE AMMASSI

PARTE NON COLLISION. — rilassamento violento
                     — phase mixing

COLLISIONALE → INFALL
CASSIEME o DOPO DM ?)

DA REVIEW SARAZIN 86 FORMAZIONE AMMASSI: PARTE GASSOSA

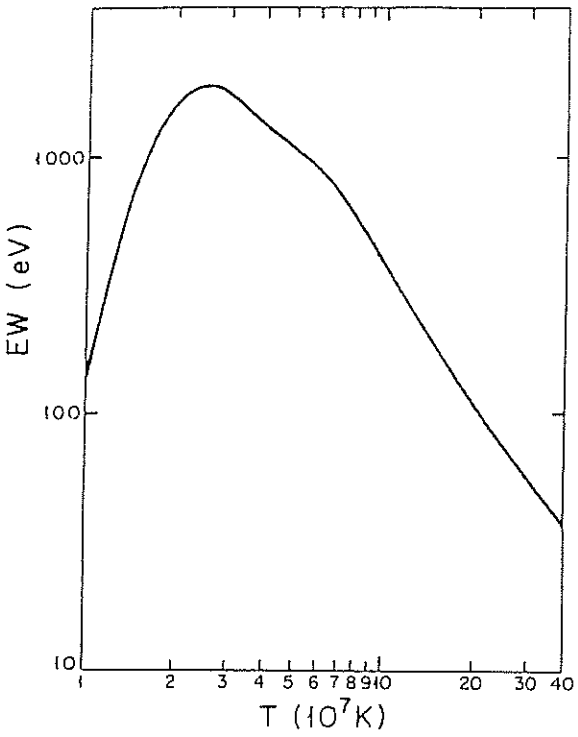

FIG. 34. The equivalent width (in eV) of the Fe K line at 7 keV as a function of gas temperature, from Bahcall and Sarazin (1978). For gas temperatures $\gtrsim 2\times10^7$ K, this is the strongest x-ray line feature.

V.B.2 above. At temperatures $T_g \gtrsim 3\times10^7$ K, the main emission mechanism is thermal bremsstrahlung, for which the total emissivity is

$$\epsilon^{ff} = 1.435\times10^{-27}\bar{g}\,T_g^{1/2} n_e \sum_i Z_i^2 n_i \text{ ergs cm}^{-3}\text{sec}^{-1}$$
$$\approx 3.0\times10^{-27} T_g^{1/2} n_p^2 \text{ ergs cm}^{-3}\text{sec}^{-1}, \quad (5.21)$$

where $\bar{g}$ is the integrated Gaunt factor, and Z_i and n_i are the charge and number density of various ions i. The second equation follows from assuming solar abundances and $\bar{g}=1.1$ in a fully ionized plasma. For $T_g \lesssim 3\times10^7$ K, line cooling becomes very important. Raymond *et al.* (1976) give the cooling rate at lower temperatures; a very crude approximation is (McKee and Cowie, 1977)

$$\epsilon \approx 6.2\times10^{-19} T_g^{-0.6} n_p^2 \text{ ergs cm}^{-3}\text{sec}^{-1},$$
$$10^5 < T_g < 4\times10^7. \quad (5.22)$$

In assessing the role of cooling in the intracluster gas, it is useful to define a cooling time scale as $t_{cool} \equiv (d\ln T_g/dt)^{-1}$. For the temperatures that apply for the intracluster gas in most clusters, Eq. (5.21) gives a reasonable approximation to the x-ray emission. If the gas cools isobarically, the cooling time is

$$t_{cool} = 8.5\times10^{10}\text{ yr}\left[\frac{n_p}{10^{-3}\text{ cm}^{-3}}\right]^{-1}\left[\frac{T_g}{10^8\text{ K}}\right]^{1/2}, \quad (5.23)$$

which is longer in most clusters than the Hubble time (age of the universe). Thus cooling is not very important in these cases. However, at the centers of some clusters the cooling time is shorter than the Hubble time, and these clusters are believed to have cooling flows (Sec. V.G).

2. Infall and compressional heating

The heating of the intracluster gas will now be considered. The major point of this discussion is that, although the gas is quite hot, no major ongoing heating of the gas is generally necessary. This is true because the cooling time in the gas is long [Eq. (5.23)], and the thermal energy in the gas is comparable to or less than its gravitational potential energy. Almost any method of introducing the gas into the cluster, either from outside the cluster or from within galaxies, will heat it to temperatures on the order of those observed.

Heating of the gas due to infall into the cluster and compression will be considered here. First, imagine that the cluster was formed before the intracluster gas fell into the cluster, and that the intracluster gas makes a negligible contribution to the mass of the cluster (Sec. III.D). If the gas was initially cold, and located at a large distance from the cluster, then its initial energy can be ignored. If the cluster potential remains fixed while the gas falls into the cluster and the gas neither loses energy by radiation nor exchanges its energy with other components of the cluster, then the total energy of the gas will remain zero. After falling into the cluster, the gas will collide with other elements of gas, and its kinetic energy will be converted to thermal energy. Thus infall and compression can produce temperatures on the order of

$$\frac{3}{2}\frac{kT_g}{\mu m_p} \approx -\phi, \quad (5.24)$$

where ϕ is the gravitational potential in the cluster. At the center of an isothermal cluster, $\phi \approx -9\sigma_r^2$, where σ_r is the line-of-sight velocity dispersion of the cluster. If this is substituted in Eq. (5.24), the derived temperature is

$$T_g \approx 5\times10^8\text{ K}\left[\frac{\sigma_r}{10^3\text{ km sec}^{-1}}\right]^2, \quad (5.25)$$

which is a factor of 5—10 times larger than the observed temperatures [Eq. (3.10)]. Of course, the gas that falls into a cluster was presumably bound to the cluster before it fell in, so that Eq. (5.25) overestimates the temperature. A similar calculation for gas bound to the cluster is given in Shibazaki *et al.* (1976).

The temperature may also be lower because of cooling during the infall, or because the gas fell in at the same time that the cluster was forming and thus experienced a

smaller potential on average. If the gas fell in at the same time that the cluster collapsed and was heated by the rapid variation of the potential during violent relaxation (Sec. II.I.2), then it might have the same energy per unit mass as the matter in galaxies,

$$\frac{3}{2}\frac{kT_g}{\mu m_p} \approx \tfrac{3}{2}\sigma_r^2 , \tag{5.26}$$

which gives Eq. (5.14) for the temperature. This is in reasonable agreement with the intracluster gas temperatures determined from x-ray spectra [Eq. (3.10)].

These crude estimates are meant only to illustrate the point that the observed gas temperatures are consistent with heating due to infall into the cluster. More detailed models for infall are discussed in Sec. V.J.1.

3. Heating by ejection from galaxies

The presence of a nearly solar abundance of iron in the intracluster gas (Secs. III.C.2 and V.B.3) suggests that a reasonable fraction of the gas may have come from stars in galaxies within the clusters. The gas ejected from galaxies is heated in two ways. First, the gas may have some energy when it is ejected. Let ϵ_{ej} be the total energy per unit mass of gas ejected from a galaxy in the rest frame of that galaxy, but not including the cluster gravitational potential, and define $3kT_{ej}/2 \equiv \mu m_p \epsilon_{ej}$. Second, the gas will initially be moving relative to the cluster center of mass at the galaxy's velocity. The ejected gas will collide with intracluster gas and thermalize its kinetic energy. On average this will give a temperature

$$kT_g \approx \mu m_p \sigma_r^2 + kT_{ej} . \tag{5.27}$$

If the ejection energy can be ignored, the temperature is given by Eq. (5.14), in reasonable agreement with the observations [Eq. (3.10)].

In a steady-state wind outflow from a galaxy, one expects $kT_{ej} \gtrsim \mu m_p \sigma_*^2$, where $\sigma_* \sim 200$ km/sec is the velocity dispersion of stars within the galaxy. If the ejection temperature is near the lower limit given by this expression, then this form of heating will not be very important because $\sigma_*^2 \ll \sigma_r^2$. However, the ejection temperature could be considerably higher. For example, supernovas within galaxies could both produce the heavy elements seen in cluster x-ray spectra and heat the gas in galaxies until it was ejected. Supernovas eject highly enriched gas at velocities of $v_{SN} \sim 10^4$ km/sec. The highly enriched, rapidly moving supernova ejecta would collide with the interstellar medium in a galaxy and heat the gas. If M_{SN} is the mass of ejecta from a supernova and M_{ej} is the resulting total gas mass ejected from the galaxy, then $T_{ej} \approx 2\times 10^9$ K $(v_{SN}/10^4$ km/sec$)^2 (M_{SN}/M_{ej})$, which will be significant if the supernova ejecta are diluted by less than a factor of about 100.

4. Heating by galaxy motions

Although ongoing heating of the intracl not be necessary to account for the observe tures, the estimates given above and the hist are sufficiently uncertain that one cannot r ing heating as an important process. One intracluster gas could be heated would be th between the gas and the galaxies that are co ing throughout the cluster (Ruderman and Hunt, 1971; Yahil and Ostriker, 1973; Sc Livio *et al.*, 1978; Rephaeli and Salpeter, 19 culation of the magnitude of this drag forc consequent heating of the intracluster gas is by the following problems. First, the motio age cluster galaxy through the intracluste likely to be just transonic $M \approx 1$, where M Mach number, v is the galaxy ve $c_s = 1480\,(T_g/10^8\ \mathrm{K})^{1/2}$ km/sec is the sound gas. If Eq. (3.10) for the observed gas tempe sumed, and the average galaxy velocity is $\sqrt{3}\sigma_r$, then the average Mach number is Thus the galaxy motion cannot be treated as highly supersonic (strong shocks, etc.) or v (incompressible, etc.). In some cases sho formed by the motion, and in some cases no s Second, the mean free path λ_i of ions in the medium due to Coulomb collisions [Eq. (5.34 to the radius of a galaxy $R_{gal} \sim 20$ kpc (Nu Thus it is unclear whether the intracluster ga treated as a collisionless gas or as a fluid, and transport processes such as viscosity (Sec. V.D tain. For example, the Reynolds number c about an object of radius R is $\mathrm{Re} \approx 3(R/$ (5.46) below], and thus is somewhat larger th $R = R_{gal}$. It is therefore uncertain whether th be laminar or turbulent. The magnetic field transport processes (Sec. V.D.3), but the coher of the field l_B estimated from Faraday rotatic tions is also comparable to the size of a galaxy (Finally, the nature of the drag force depends c the galaxy contains interstellar gas or not. If contains no gas, it affects the intracluster me through its gravitational field. If the galax high-density gas, it can give the galaxy an effe face. For example, a gasless galaxy in superson probably will not produce a bow shock, while a galaxy may (Ruderman and Spiegel, 1971; Hu Gisler, 1976).

It is convenient to write the rate of energy lc galaxy and the heating rate of the intracluster me

$$\frac{dE}{dt} = \pi R_D^2 \rho_g v^3 ,$$

where ρ_g is the intracluster gas density and R_D fective radius of the galaxy for producing the dr First, assume that the intracluster gas is coll Then the drag is given by the dynamical friction Eq. (2.34) and